© 2021. Published by The Company of Biologists Ltd | Development (2021) 148, dev196147. doi:10.1242/dev.196147

RESEARCH ARTICLE

Brahma-related gene 1 has time-specific roles during brain and eye development

Dörthe Holdhof[1,2], Melanie Schoof[1,2], Sina Al-Kershi[1,2], Michael Spohn[2,3], Catena Kresbach[1,2], Carolin Göbel[1,2], Malte Hellwig[1,2], Daniela Indenbirken[4], Natalia Moreno[5], Kornelius Kerl[5] and Ulrich Schüller[1,2,6,*]

ABSTRACT

During development, gene expression is tightly controlled to facilitate the generation of the diverse cell types that form the central nervous system. Brahma-related gene 1 (*Brg1*, also known as *Smarca4*) is the catalytic subunit of the SWItch/sucrose nonfermentable (SWI/SNF) chromatin remodeling complex that regulates transcription. We investigated the role of *Brg1* between embryonic day 6.5 (E6.5) and E14.5 in *Sox2*-positive neural stem cells (NSCs). Being without major consequences at E6.5 and E14.5, loss of *Brg1* between E7.5 and E12.5 resulted in the formation of rosette-like structures in the subventricular zone, as well as morphological alterations and enlargement of neural retina (NR). Additionally, *Brg1*-deficient cells showed decreased survival *in vitro* and *in vivo*. Furthermore, we uncovered distinct changes in gene expression upon *Brg1* loss, pointing towards impaired neuron functions, especially those involving synaptic communication and altered composition of the extracellular matrix. Comparison with mice deficient for integrase interactor 1 (*Ini1*, also known as *Smarcb1*) revealed that the enlarged NR was *Brg1* specific and was not caused by a general dysfunction of the SWI/SNF complex. These results suggest a crucial role for *Brg1* in NSCs during brain and eye development.

KEY WORDS: Brg1 (Smarca4), SWI/SNF complex, Brain, Eye, Development, Mouse

INTRODUCTION

The development of the central nervous system (CNS) is a complex series of events. In brief, the neural tube is formed around embryonic day 8.5 (E8.5) in mice, followed by the formation of the primary vesicles (prosencephalon, mesencephalon and rhombencephalon) at E9.0 and subsequently of the secondary vesicles (telencephalon, diencephalon, mesencephalon, metencephalon and myelencephalon). In the cerebral cortex, neurogenesis is finished around E18.5, whereas cerebellar development is not finalized until postnatal day 21 (P21) (Chen et al., 2017). Spatiotemporal changes in gene expression in multipotent stem cells are the prerequisites for the development of distinct cell types that make up the CNS (Panamarova et al., 2016). Partially, this is facilitated by epigenetic regulators like the SWItch/sucrose nonfermentable [SWI/SNF, BRG1/BRM-associated factor (BAF)] chromatin remodeling complexes. These are multi-subunit complexes that use ATP hydrolysis to mobilize nucleosomes in order to regulate transcription (Kwon et al., 1994; Wang et al., 1996; Hargreaves and Crabtree, 2011). In total, about 29 genes encode for components that can be combined in a modular manner to form cell type-specific SWI/SNF complexes (Alpsoy and Dykhuizen, 2018; Mashtalir et al., 2018). For example, different SWI/SNF complex compositions have been described for embryonic stem cells (esBAF), neural progenitors (npBAF) and post-mitotic neurons (nBAF) (Lessard et al., 2007; Ho et al., 2009). Mutations in one or more subunits might lead to the expression of an altered SWI/SNF complex with aberrant functions that contribute to the development of diseases such as cancer (Dutta et al., 2017; Sen et al., 2017). Brahma-related gene 1 (*Brg1*, also known as *Smarca4* and *Baf190a*) is one of the two mutually exclusive ATPase subunits of the SWI/SNF complex (Chiba et al., 1994; Wang et al., 1996). In humans, *BRG1* mutations have been found in individuals suffering from intellectual disability disorders such as Coffin-Siris syndrome (Tsurusaki et al., 2012; Holsten et al., 2018; Sekiguchi et al., 2019; Li et al., 2020). Additionally, *BRG1* has been proposed to play an important role in the pathogenesis of autism spectrum disorders (De Rubeis et al., 2014; Lim et al., 2017). However, mutations in this gene have also been identified in diverse tumor entities, such as rhabdoid tumors and small cell carcinoma of the ovary of the hypercalcemic type (SCCOHT), indicating a tumor-suppressive role (Hasselblatt et al., 2014; Lang and Hendricks, 2018; Holdhof et al., 2021). The presence of *BRG1* mutations in these different diseases suggests a context-specific role of this transcriptional regulator. Mouse models have been used to better characterize the role of *Brg1* in normal development and disease. Previous studies revealed that *Brg1* is indispensable very early in embryonic development, as homozygous knockout mice die during peri-implantation stage (Bultman et al., 2000). In contrast, a heterozygous *Brg1* loss results in a predisposition to mammary tumors and exencephaly (Bultman et al., 2008). *Brg1* is constantly expressed during neural development and is involved in processes like self-renewal of neural stem cells (NSCs) and proper formation of all major brain structures (Machida et al., 2001; Lessard et al., 2007; Moreno et al., 2014; Holdhof et al., 2020). Additionally, the ATPase is essential for Schwann cell differentiation but less important for oligodendrocyte differentiation (Weider et al., 2012; Bischof et al., 2015). Altogether, these mouse models support the hypothesis of a context-dependent role of *Brg1*.

In the present study, we investigated the function of *Brg1* during the different stages of embryonic CNS development. For this purpose, we generated *Sox2-creER^{T2}::Brg1$^{fl/fl}$* mice and induced the

[1]Department of Pediatric Hematology and Oncology, University Medical Center Hamburg-Eppendorf, 20246 Hamburg, Germany. [2]Research Institute Children's Cancer Center Hamburg, 20251 Hamburg, Germany. [3]Bioinformatics Facility, University Medical Center, Hamburg-Eppendorf, 20246 Hamburg, Germany. [4]Heinrich-Pette-Institute, Leibniz Institute for Experimental Virology, 20251 Hamburg, Germany. [5]Department of Pediatric Hematology and Oncology, University Children's Hospital Münster, 48149 Münster, Germany. [6]Institute of Neuropathology, University Medical Center Hamburg-Eppendorf, 20246 Hamburg, Germany.

*Author for correspondence (u.schueller@uke.de)

D.H., 0000-0003-4664-3848; U.S., 0000-0002-8731-1121

Handling Editor: Paola Arlotta
Received 17 August 2020; Accepted 4 May 2021

Development (2021) 148, dev196147. doi:10.1242/dev.196147

loss of *Brg1* expression in Sex determining region Y (SRY) box 2 (*Sox2*)-positive NSCs at defined times by tamoxifen administrations. We chose the period between E6.5 and E14.5 to cover developmental stages starting immediately before neural tube formation until the peak of neurogenesis in the cerebral cortex (Martynoga et al., 2012; Chen et al., 2017). Overall, our study highlights the importance of *Brg1* for brain and eye development as well as its time-specific role as a transcriptional regulator.

RESULTS

Loss of *Brg1* between E7.5 and E12.5 results in morphological alterations in the CNS

In order to elucidate time-specific roles of *Brg1* in NSCs, we generated *Sox2-creER^{T2}::Brg1$^{fl/fl}$* mice. Here, Cre-mediated recombination of the loxP sites in the conserved ATPase/Helicase motifs of *Brg1* results in an instable mRNA causing a loss of the BRG1 protein (Fig. 1A). We introduced *Brg1* deficiency with administration of a single dose of tamoxifen between E6.5 and E14.5 (Fig. 1B), and analyzed their brains by Hematoxylin and Eosin staining between E14.5 and E21.5 (Fig. 1C-M).

Sox2-creER^{T2}::Brg1$^{fl/fl}$ embryos presented morphological alterations in the brain with varying penetrance when the loss of *Brg1* was induced between E7.5 and E12.5 (Fig. 1C). In contrast, induction of *Brg1* deficiency at E6.5 or E14.5 did not alter normal prenatal brain development (Fig. 1C,F,G,L). In detail, all *Sox2-creER^{T2}::Brg1$^{fl/fl}$* embryos with *Brg1* deletion at E7.5 developed a lesion close to the basal part of the cerebrum (Fig. 1H,I,M). Based on morphology, it resembled neural retina (NR) (Fig. 1Hii,Ii) that was altered in the embryonic eye of E18.5 mutant mice (Fig. 1I, arrow). About 63% of these mice showed additional abnormalities in the subventricular zone (SVZ), often with rosette-like structures (Fig. 1Iii,M). After *Brg1* deprivation at E8.5, *Sox2-creER^{T2}::Brg1$^{fl/fl}$* embryos similarly showed features like the NR-like lesion (70%) or the involvement of the SVZ (80%) (Fig. 1M). However, in case of an induced *Brg1* loss at E9.5, the alterations were mainly located in the SVZ (88%) and the cerebral cortex (12%). Furthermore, the embryos presented with hydrocephalus (12%) or with a combination of these phenotypes (Fig. 1J,K,M). The abnormalities in the SVZ usually involved rosette-like structures, and the layering of the cerebral cortex seemed disturbed, as shown in Hematoxylin and Eosin stains at E14.5 or E18.5 (Fig. 1Ji,Ki,Kii). Furthermore, the NR presented with rosettes in some animals (Fig. 1Jii). Initiation of *Brg1* loss at E10.5 or E12.5 primarily resulted in a disrupted SVZ with rosette-forming structures (73% and 100% of embryos, respectively), very similar to those observed after *Brg1* disruption at E9.5 (Fig. 1M).

In order to examine whether the brain regions with architectural disruptions were formed by cells that had lost *Brg1*, we used immunohistochemistry (IHC) to detect expression of the protein at the cellular level (Fig. S1). Overall, even though there were different morphological alterations found in the embryonic brain after loss of *Brg1* at E7.5 and E9.5 in *Sox2*-expressing NSCs, the abundance of BRG1-negative cells (Fig. S1F-N, yellow arrow) was similar. BRG1-deficient cells were randomly scattered in the neocortex and the thalamic regions, whereas the SVZ, including the rosette-like structures, was mainly BRG1 competent. The NR-like region close to the basal cerebrum in embryos that had lost *Brg1* at E7.5 harbored many BRG1-negative cells (Fig. S1J).

Taken together, *Brg1* deficiency induced between E7.5 and E12.5 in *Sox2*-expressing cells causes architectural alterations in the embryonic brain. The type of abnormality depends on the time of *Brg1* deprivation, as the NR-resembling lesion close to the basal cerebrum only occurred after *Brg1* loss at E7.5 or E8.5. However, alterations in the SVZ were found after *Brg1* deprivation between E7.5 and E12.5, indicating that the cells forming the SVZ are dependent on proper *Brg1* expression for a longer period.

Loss of *Ini1* at E9.5 disrupts the architecture of the SVZ similar to *Brg1* deprivation

Next, we were interested in whether the morphological alterations in the brains of *Sox2-creER^{T2}::Brg1$^{fl/fl}$* embryos were specific to *Brg1* or the result of a non-functional SWI/SNF complex. We generated *Sox2-creER^{T2}::Ini1$^{fl/fl}$* embryos and investigated the influence of an *Ini1* deficiency induced at E7.5 or E9.5, as INI1 is another subunit of the majority of SWI/SNF complexes (Alpsoy and Dykhuizen, 2018). After induction of *Ini1* deprivation at E7.5, brains appeared normal at E14.5 and E18.5 (Fig. 2A-D). We did not observe any alterations in the SVZ or the neocortex, nor did we detect any NR-resembling structure (Fig. 2Ci,Cii,Di,Dii) as we did in the brains of *Sox2-creER^{T2}::Brg1$^{fl/fl}$* embryos (Fig. 1Hii,Ii,Iii). In contrast, loss of *Ini1* at E9.5 caused formation of rosette-like structures in the SVZ in 7/12 embryos (58%) that resembled those found in the SVZ of *Brg1*-deficient embryos (Fig. 1Ji,Kii and Fig. 2Ei,Fii). The neocortex appeared without major alterations in the analyzed animals (Fig. 2Fi). Of note, the pattern of INI1-negative cells in *Sox2-creER^{T2}::Ini1$^{fl/fl}$* embryos (Fig. S1O-Z) at E18.5 was similar to that of BRG1 deprived cells in *Sox2-creER^{T2}::Brg1$^{fl/fl}$* embryos (Fig. S1B-N).

Overall, we suggest that some morphological alterations that we observed upon loss of *Brg1* in *Sox2-creER^{T2}::Brg1$^{fl/fl}$* embryos were caused by a non-functional SWI/SNF complex. However, other abnormalities, especially the NR-resembling cell accumulation, were specific to the lack of *Brg1*.

Brg1 deficiency enhances apoptosis

Subsequently, we examined whether the phenotypic alterations we observed between E14.5 and E18.5 were a direct consequence of the BRG1 protein loss. Therefore, we examined E10.5 and E12.5 embryos after *Brg1* deletion at E7.5 and E12.5, respectively. Macroscopically, *Sox2-creER^{T2}::Brg1$^{fl/fl}$* embryos of both stages (Fig. 3C,Q) appeared normal in comparison with their *Brg1$^{fl/fl}$* littermates (Fig. 3A,O). Tamoxifen-induced *Brg1* loss at E7.5 caused no obvious morphological alterations in Hematoxylin and Eosin stains (Fig. 3B,D,E,G) even though the protein was lost in a substantial number of cells (Fig. 3F,H). As the number of BRG1 negative cells was higher compared with E18.5 brains (Fig. S1), we speculated that *Brg1* deficiency caused a decrease in proliferation and/or an increase in apoptosis. Therefore, we stained for phosphorylated histone H3 (pHH3) and cleaved Caspase 3 (clCasp3) to examine the number of proliferating and apoptotic cells, respectively. The proportion of pHH3-positive cells was equal in *Brg1$^{fl/fl}$* (Fig. 3I) and *Sox2-creER^{T2}::Brg1$^{fl/fl}$* brains (Fig. 3K,M). In contrast, we observed a significant increase in clCasp3-expressing cells in the CNS of *Brg1*-deprived animals (Fig. 3L) compared with controls (Fig. 3J,N). We compared proliferation and apoptosis in different brain regions and determined that the changes in apoptosis were especially pronounced in the midbrain regions (Fig. S2A-G). Furthermore, following *Brg1* loss at E7.5, we observed many clCasp3-positive cells in regions harboring increased numbers of BRG1-negative cells in brains of *Sox2-creER^{T2}::Brg1$^{fl/fl}$* animals at E12.5 (Fig. S2H-O).

After loss of *Brg1* at E9.5, there were no morphological differences detectable in Hematoxylin and Eosin stains of *Brg1$^{fl/fl}$* (Fig. 3P,S) and *Sox2-creER^{T2}::Brg1$^{fl/fl}$* brains (Fig. 3R,U). There were few BRG1-deficient cells in the ganglionic eminence but no significant alterations in proliferation or apoptosis, as indicated by quantification of pHH3-expressing (Fig. 3W,Y,AA) or

Development (2021) 148, dev196147. doi:10.1242/dev.196147

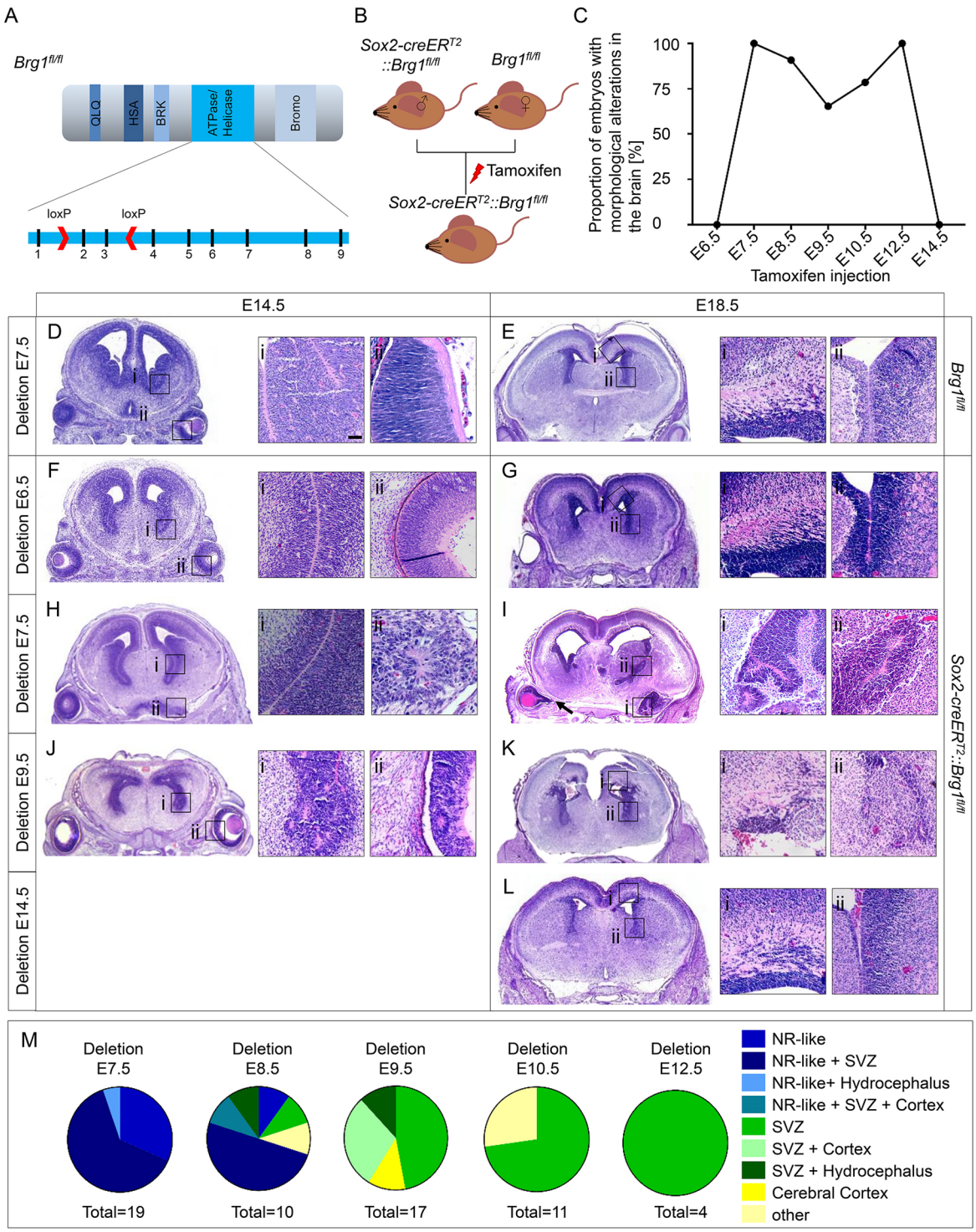

Fig. 1. Experimental design and overview of main phenotypes observed in *Sox2-creER^{T2}::Brg1$^{fl/fl}$* mice. (A) In *Brg1$^{fl/fl}$* mice, loxP sites are located upstream of exon 2 and downstream of exon 3 of the catalytic domain. (B) Male *Sox2-creER^{T2}::Brg1$^{fl/fl}$* mice and female *Brg1$^{fl/fl}$* mice were crossed, and pregnant mice were injected with a single dose of tamoxifen between E6.5 and E14.5. (C) Mutant embryos presented with morphological abnormalities only when *Brg1* was deleted between E7.5 and E12.5, and with varying penetrance of the phenotypic alterations. (D,E) Hematoxylin and Eosin stains of *Brg1$^{fl/fl}$* frontal brain sections at E14.5 (D) and E18.5 (E) serve as controls. (Di-Eii) High-power images (100× magnification) of the SVZ (Di,Eii), the neural retina (NR) (Dii) and the neocortex (Ei) are shown. (F-Gii,L-Lii) Overview and high-power (100× magnification) images of Hematoxylin and Eosin stains of *Sox2-creER^{T2}::Brg1$^{fl/fl}$* embryos do not show any morphological abnormalities after loss of *Brg1* at E6.5 (F-Fii,G-Gii) or E14.5 (L-Lii). (H-Hii) After loss of *Brg1* at E7.5, the SVZ appears normal at E14.5 (Hi), whereas the cells close to the third ventricle are architecturally disturbed (Hii). (I-Iii) At E18.5, organizational alterations in the SVZ (Ii) and a cell accumulation close to the basal cerebrum (Iii) are present (I). (J-Kii) Deprivation of *Brg1* at E9.5 results in rosette-like structures in the SVZ (J,Ji,Kii) and the NR (Jii), as well as alterations in the neocortex (K,Ki). (M) Type and localization of morphological alterations are dependent on the time point of *Brg1* deletion. Embryos between E14.5 and E21.5 were analyzed in C and M. Frontal sections of whole-embryo heads are shown in D-L. Scale bar: 50 µm in Di for Di-Lii. Arrow in I indicates morphological alterations in the eye. *n*=6, *n*=19, *n*=11, *n*=26, *n*=14, *n*=4 and *n*=3 *Sox2-creER^{T2}::Brg1$^{fl/fl}$* embryos were analyzed after *Brg1* loss at E6.5, E7.5, E8.5, E9.5, E10.5, E12.5 and E14.5, respectively.

Development (2021) 148, dev196147. doi:10.1242/dev.196147

clCasp3-expressing (Fig. 3X,Z,AB) cells. In conclusion, our data suggest that introducing *Brg1* deficiency in *Sox2*-expressing cells at E7.5 results in an increase of apoptosis.

Loss of *Brg1* at E7.5 hinders proper eye formation

The cell accumulation attached to the basal cerebrum present in *Sox2-creER^{T2}::Brg1$^{fl/fl}$* embryos after *Brg1* loss at E7.5 resembled NR in Hematoxylin and Eosin stains (Fig. 1Ii). Therefore, we compared the NR-like structure with NR of healthy controls by IHC marker expression (Fig. 4A-N). At E18.5, mainly two retinal layers are visible, the neuroblast layer (NBL) and the ganglion cell layer (GCL). Both were easily recognizable in Hematoxylin and Eosin stains of retina in healthy controls (Fig. 4B). Based on morphology, the NR-like in *Sox2-creER^{T2}::Brg1$^{fl/fl}$* embryos showed similar structures resembling NBL and GCL (Fig. 4I). Accordingly, SOX2, a marker for retinal progenitor cells (Saha et al., 2018) was found in both the NBL of controls and the NBL-resembling structure in *Brg1*-deprived animals (Fig. 4C,J). Similarly, expression of paired box protein 6 (PAX6), orthodenticle homeobox 2 (OTX2), oligodendrocyte transcription factor 2 (OLIG2) and neuron-specific class III beta-tubulin (TUJ1) was comparable in the NR of controls (Fig. 4D-G) and the NR-resembling structure of *Brg1*-deficient mice (Fig. 4K-N).

Based on this comparison, we concluded that the structure at the basal cerebrum was in fact expanded NR. Next, we investigated at which embryonic stage the enlarged NR occurred. Therefore, we examined embryonic eyes between E12.5 and E18.5 (Fig. 4O-V). First alterations became visible at E16.5 in *Sox2-creER^{T2}::Brg1$^{fl/fl}$* embryos, with the NR being present in multiple folds. Hence, we concluded that *Brg1* deficiency at E7.5 results in the formation of an expanded NR, which occurs after E14.5.

Neurosphere formation *in vitro* is dependent on *Brg1*

In order to characterize the fate of *Brg1* deficient cells, we generated *Sox2-creER^{T2}::lslRFP$^{fl/fl}$* and *Sox2-creER^{T2}::Brg1$^{fl/fl}$::lslRFP$^{fl/fl}$* mice. The *lslRFP* transgene in these mice harbors a 'transcriptional stopper' element flanked by loxP sites upstream of the red fluorescent protein (RFP)-encoding sequence (Luche et al., 2007). Consequently, all cells and their progeny, in which the Cre recombinase has been activated by tamoxifen, are marked by RFP expression (Fig. 5A). RFP-expressing cells were isolated using a fluorescence-activated cell sorting (FACS) and used for neurosphere assays.

Brg1 loss significantly decreased the yield of cells that were obtained from E14.5 brains (Fig. 5B). After tamoxifen exposure at E7.5 and E9.5, only 7.4% and 2.8% of cells from *Sox2-creER^{T2}::Brg1$^{fl/fl}$::lslRFP$^{fl/fl}$* brains were RFP positive, respectively. In comparison, 15.4% and 8.0% RFP-positive cells were isolated from *Sox2-creER^{T2}::lslRFP$^{fl/fl}$* embryos after tamoxifen treatment at E7.5 and E9.5, respectively. To validate the efficiency of the system, we performed BRG1 immunofluorescence (IF) immediately after FACS (Fig. 5C). For both time points of tamoxifen injections, only 48-86% of RFP-positive cells were negative for BRG1 (data not shown). This suggested that the efficiency of the Cre enzyme is reduced, when two floxed transgenes (here *Brg1$^{fl/fl}$* and *lslRFP$^{fl/fl}$*) are recombined simultaneously.

Next, we cultured the RFP-positive cells to investigate their ability to form neurospheres. After 7 days, neurospheres were present in the wells of all four conditions (Fig. 5D). However, in wells with cells derived from *Sox2-creER^{T2}::Brg1$^{fl/fl}$::lslRFP$^{fl/fl}$* brains, there were significantly fewer spheres found (Fig. 5E). After tamoxifen at E7.5, the number of neurospheres was reduced by 92% and after tamoxifen at E9.5 it was reduced by 84%. Moreover, IF staining revealed that the neurospheres contained almost exclusively BRG1-positive cells (Fig. 5F). This suggests that *Brg1*-expressing cells are selected in culture, whereas *Brg1* deficiency hinders the formation of neurospheres. Taken together, loss of *Brg1* at either E7.5 or E9.5 decreases the abundance of the respective cells at E14.5. Furthermore, these cells are not able to form neurospheres *in vitro*.

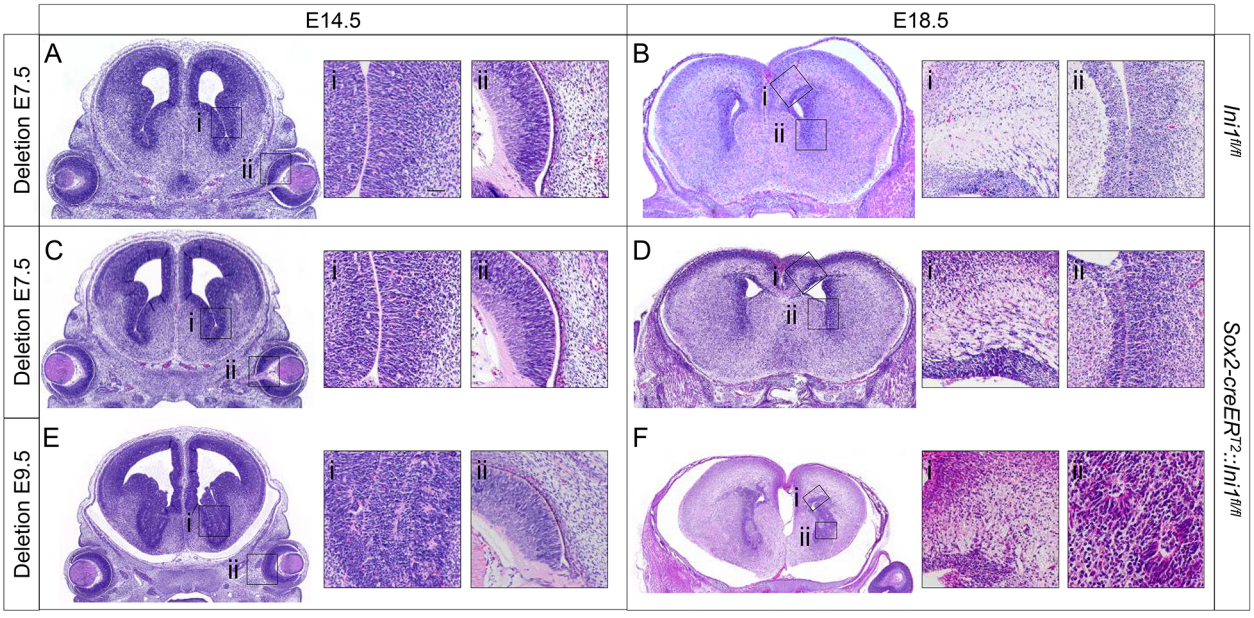

Fig. 2. *Ini1* deficiency induced at E9.5 in *Sox2*-expressing cells results in a similar phenotype as loss of *Brg1*. (A,B) Hematoxylin and Eosin stains of *Ini1$^{fl/fl}$* frontal brain sections at E14.5 (A) and E18.5 (B) serve as controls. (Ai-Bii) High-power images (100× magnification) of the SVZ (Ai,Bii), the NR (Aii) and the neocortex (Bi) are shown. (C-Dii) Loss of *Ini1* at E7.5 (C,D) causes no morphological abnormalities until E18.5 in the brain, including SVZ and neocortex or the eyes of *Sox2-creER^{T2}::Ini1$^{fl/fl}$* embryos (Ci-Dii). (E-Fii) Induction of *Ini1* deprivation at E9.5 (E,F) results in rosette-like structures in the SVZ (Ei,Fii), whereas the eye and neocortex appear normal (Eii,Fi). Frontal sections of whole-embryo heads are shown in A-F. Scale bar: 50 µm in Ai for Ai-Fii. *n*=7 and *n*=12 *Sox2-creER^{T2}::Ini1$^{fl/fl}$* embryos were analyzed after *Brg1* deletion at E7.5 and E9.5, respectively.

Development (2021) 148, dev196147. doi:10.1242/dev.196147

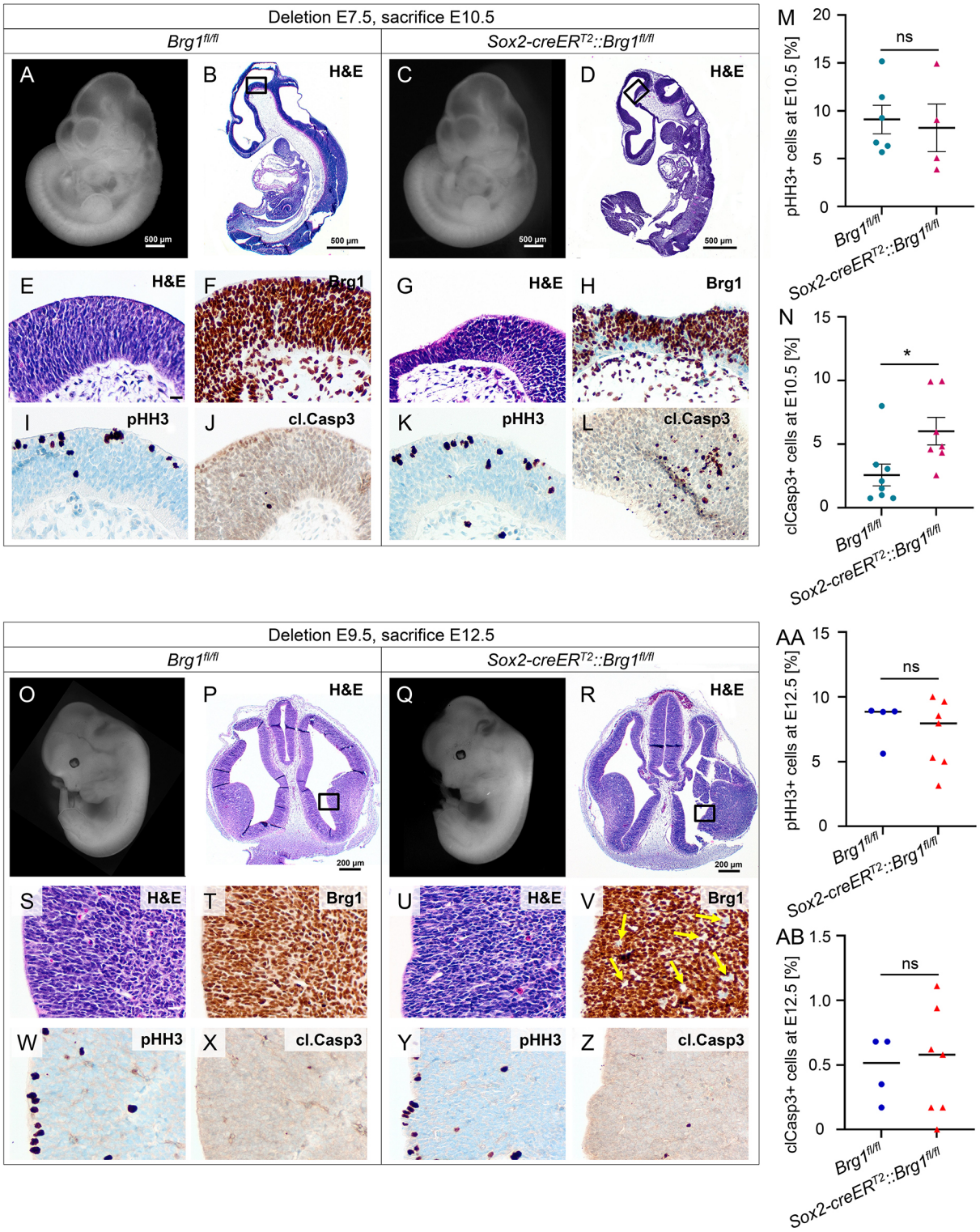

Fig. 3. Loss of *Brg1* at E7.5 enhances apoptosis at E10.5. (A-D) Macroscopic (A,C; 10× magnification) and Hematoxylin and Eosin images (B,D) at E10.5 of *Brg1*$^{fl/fl}$ and *Sox2-creER*^{T2}*::Brg1*$^{fl/fl}$ after *Brg1* loss at E7.5 are shown. (E-N) High-power images (200× magnification) of the same embryos with Hematoxylin and Eosin (E,G), BRG1 (F,H), pHH3 (I,K) and cl.Casp3 (J,L) staining, as well as quantification of pHH3^{+} (M) and clCasp3+ cells (N) are depicted. (O-R) Macroscopic (O,Q) and frontal Hematoxylin and Eosin (P,R) images at E12.5 of *Brg1*$^{fl/fl}$ and *Sox2-creER*^{T2}*::Brg1*$^{fl/fl}$ after tamoxifen at E9.5 are shown. (S-AB) High-power images (200× magnification) of the same embryos of Hematoxylin and Eosin (S,U), Brg1 (T,V), pHH3 (W,Y) and cl.Casp3 (X,Z) staining as well as quantification of pHH3^{+} (AA) and clCasp3^{+} cells (AB) suggest no differences in mutants. Data are mean±s.e.m. ns, not significant; *P<0.05; n≥3 animals. Arrows in V indicate BRG1-negative cells. In B,D,P and R, the areas outlined are shown at higher magnification in the images below. Scale bars: 20 µm in E-L,S-Z.

Development (2021) 148, dev196147. doi:10.1242/dev.196147

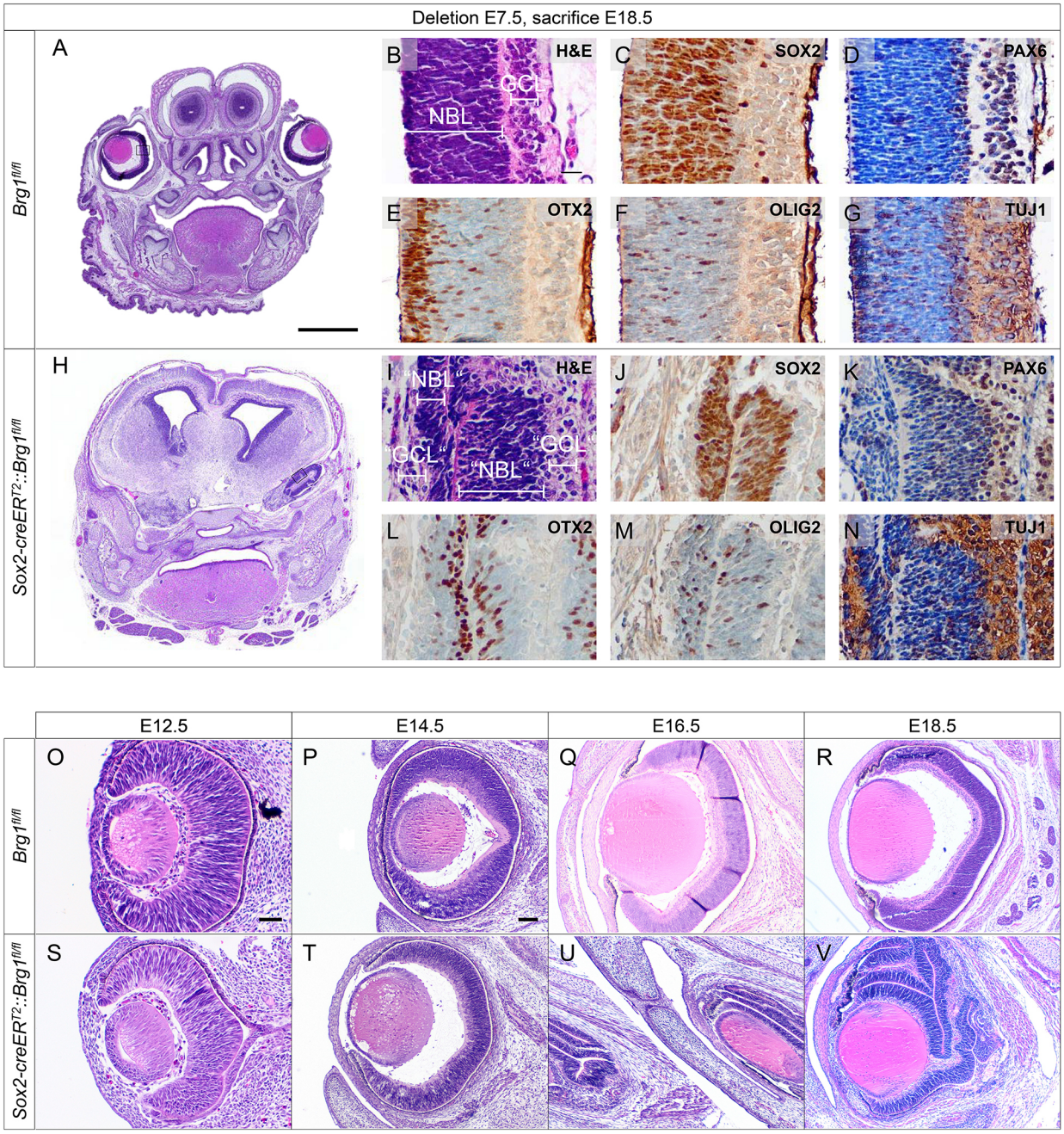

Fig. 4. *Brg1* deletion at E7.5 causes formation of an enlarged retina. (A,B,H,I) Comparison of NR of a healthy control (A,B) and the NR resembling cell accumulation (H,I) at E18.5 reveals morphological similarities in Hematoxylin and Eosin stains. Neuroblast layer (NBL) and ganglion cell layer (GCL), as well as NBL-like and GCL-like structures are marked in Hematoxylin and Eosin stains of *Brg1*$^{fl/fl}$ retina (B) and in the cell accumulation of *Sox2-creER*^{T2}*::Brg1*$^{fl/fl}$ embryos (I). (C-G,J-N) Expression patterns of SOX2 (C,J), PAX6 (D,K), OTX2 (E,L), OLIG2 (F,M) and TUJ1 (G,N) in *Brg1*$^{fl/fl}$ and *Sox2-creER*^{T2}*::Brg1*$^{fl/fl}$ mice indicate similarities. Histological images in A-N show representative regions of E18.5 heads at 200× magnification. (O-V) Hematoxylin and Eosin sections of the indicated ages suggesting that the phenotype in *Sox2-creER*^{T2}*::Brg1*$^{fl/fl}$ embryos is visible after E14.5 [100× (O,S) or 40× (P-R,T-V) magnification]. All images display embryos with *Brg1* loss at E7.5. Scale bars: in A, 1000 µm for A,H; in B, 20 µm for B-G,I-N; in O, 50 µm for O,S; in P, 100 µm for P-R,T-V. $n \geq 3$ animals.

Brg1 is essential for expression of genes related to neuronal function and the extracellular matrix

We performed RNA-sequencing to analyze global changes in gene expression upon loss of *Brg1*. We used the same experimental set-up as for the neurosphere assay and isolated the RNA immediately after FACS (Fig. 5A).

Unsupervised hierarchical clustering of significant differentially expressed genes (DEGs) defined by FDR<0.1 and log2 fold change >±0.6 revealed four distinct clusters (Fig. 5G). These clusters corresponded with the four treatment groups: *Sox2-creER*^{T2}*::Brg1*$^{fl/fl}$*::lslRFP*$^{fl/fl}$ and *Sox2-creER*^{T2}*::lslRFP*$^{fl/fl}$ embryos, with *Brg1* disruption either at E7.5 or at E9.5. We identified 172 and 18 downregulated, as well as 115 and 97 upregulated genes upon *Brg1* loss at E7.5 and E9.5, respectively (Fig. S3A,B). In order to interpret these results functionally, we performed gene ontology (GO) term enrichment analyses. Significantly enriched terms involving DEGs

Development (2021) 148, dev196147. doi:10.1242/dev.196147

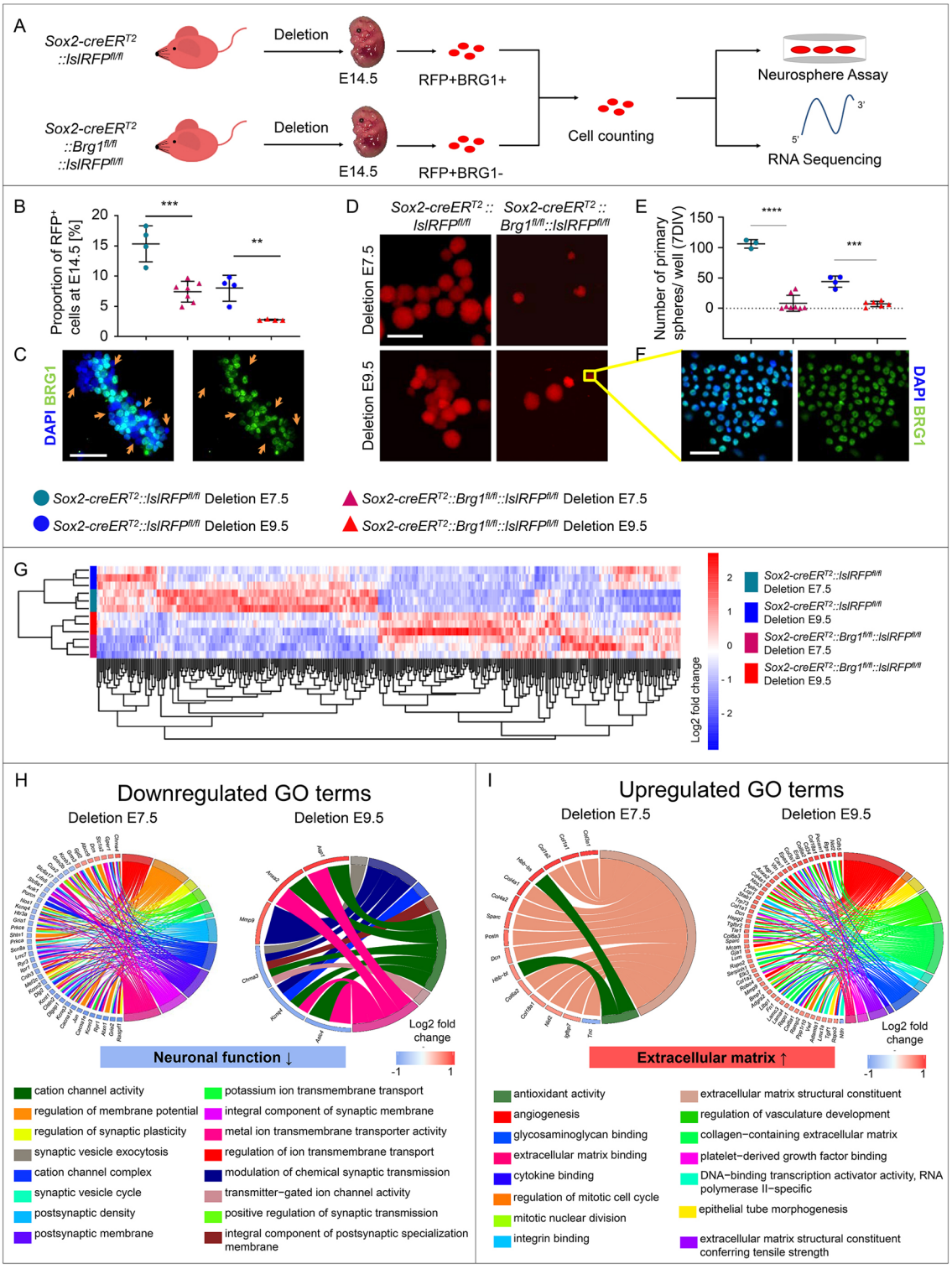

Fig. 5. Loss of *Brg1* decreases cell survival and causes time-specific changes in gene expression. (A) Experimental set-up for the investigation of Brg1-deficient cells by a neurosphere assay and transcriptome analysis is depicted. (B) The yield of RFP-positive cells is reduced in *Sox2-creER^{T2}::Brg1$^{fl/fl}$::RFP$^{fl/fl}$* compared with *Sox2-creER^{T2}::lslRFP$^{fl/fl}$* embryos. (C) In *Sox2-creER^{T2}::Brg1$^{fl/fl}$::RFP$^{fl/fl}$* embryos, the RFP-expressing cell populations consist of Brg1-positive and Brg1-negative cells. (D,E) Cells derived from both *Sox2-creER^{T2}::lslRFP$^{fl/fl}$* and *Sox2-creER^{T2}::Brg1$^{fl/fl}$::RFP$^{fl/fl}$* form neurospheres after 7 days *in vitro* (D), but the number of neurospheres is reduced in the latter (E). (F) Only BRG1-competent cells form neurospheres, as indicated by immunofluorescent staining. (G) Hierarchical cluster analysis of the differentially expressed genes (DEGs) reveals four distinct transcriptional clusters. (H,I) GO chords of significantly enriched regulated gene ontology (GO) terms after loss of *Brg1* at E7.5 or E9.5 depict involved DEGs sorted according to log2 fold change on the left side and GO terms on the right side of each circle. Immunofluorescent staining in C and F show representative images of *Sox2-creER^{T2}::Brg1$^{fl/fl}$::RFP$^{fl/fl}$* derived cells/neurospheres after tamoxifen at E9.5 (Brg1, green nuclei; DAPI, blue nuclei) at 200× magnification. Scale bars: 50 µm in C,F; 200 µm in D. Orange arrows in C indicate Brg1-negative cells. $n \geq 3$ animals. Data are mean±s.d. $^{**}P<0.01$, $^{***}P<0.001$ and $^{****}P<0.0001$. Color scales in G-I indicate the log2 fold change of DEGs.

Development (2021) 148, dev196147. doi:10.1242/dev.196147

with a log2 fold change >±0.6 were visualized as GOchords (Fig. 5H,I). Functionally related terms were summarized as their lowest common denominator derived from the 10 most significant terms per category (i.e. 'Molecular Function', 'Cellular Component' and 'Biological Process'). In the GOchords, the respective GO terms are shown on the right half of the circle, connected by chords to the involved DEGs, which are depicted on the left side of the circle. Loss of *Brg1* at both investigated time points (E7.5 and E9.5) resulted in downregulation of the GO terms 'cation channel complex' (GO: 0034703) and 'metal ion transmembrane transporter activity' (GO: 0046873). The other GO terms downregulated upon *Brg1* loss differed between the groups. Still, all downregulated GO terms were related to the function of neurons; in particular, to their ability to form synaptic cell-cell communications. This indicates that NSCs are dependent on *Brg1* to give rise to functional neurons, irrespective of the time point.

Using this method to identify enriched GO terms upon *Brg1* loss at E7.5 resulted in only two upregulated GO terms: 'antioxidant activity' (GO: 0016209) and 'extracellular matrix structural constituent' (GO: 00052011) (Fig. 5I). However, when *Brg1* deficiency was introduced at E9.5, several GO terms were upregulated, including processes involved in cell cycle, vascular development and extracellular matrix (ECM) functions. Next, we performed Kyoto Encyclopedia of Genes and Genomes (KEGG) pathway analysis. The results matched to the GO term analysis, because terms like 'GABAergic synapse' or 'Focal adhesion' were altered irrespective of the time of *Brg1* loss, whereas the *Brg1* deficiency induced at E9.5 altered additional pathways, including 'cell cycle', 'DNA replication' or 'PI3K-Akt signaling pathway' (Fig. S4).

Genes encoding collagens were significantly upregulated due to *Brg1* deprivation at E7.5 and at E9.5. Additionally, after *Brg1* loss at E9.5, further genes encoding other ECM components such as vitronectin, fibronectin 1, heparan sulfate proteoglycan 2 (*Hspg2*, perlecan), laminin α4 (*Lama4*) and laminin γ3 (*Lamc3*) were significantly upregulated. Concordantly, as laminins and integrins interact (Belkin and Stepp, 2000), integrin α1 expression was also enhanced. Other upregulated DEGs involved genes such as the stem cell marker nestin, *Bmp7* or Tgfβ receptor II (*Tgfbr2*). Consistently, clustering of KEGG pathway TGFβ signaling pathway (mmu04359) genes was according to genotype (Fig. S5A), but did not result in enhanced phosphorylated Smad1,5,8 (p-Smad 1,5,8) reactivity in IF (immunofluorescence staining) (Fig. S5B-F).

We also used the transcriptome data to examine whether and how loss of *Brg1* influenced the expression of other SWI/SNF complex members (Fig. S6) present in the complex in NSCs (Lessard et al., 2007). Expression of the alternative ATPase subunit (*Smarca2*) was significantly (FDR<0.1) lower, irrespective of the time of *Brg1* loss.

Taken together, *Brg1* deprivation at either E7.5 or E9.5 results in the downregulation of genes related to the function of neurons and upregulation of genes and GO terms associated with the ECM. However, *Brg1* loss at E7.5 mainly causes enhanced expression of collagen-encoding genes, whereas *Brg1* deficiency at E9.5 additionally increases a variety of other ECM-related genes.

Loss of *Brg1* at E7.5 hinders proper eye formation

As analysis of GO term enrichment identified only two upregulated GO terms that merely included 15/115 (13%) of the DEGs upon *Brg1* loss at E7.5, we took a closer look at the individual upregulated DEGs (Fig. 6A). We recognized many genes that are expressed during eye development, including fibroblast growth factor 15 (*Fgf15*), pituitary homeobox 2 (*Pitx2*), *Otx2*, Iroquois homeobox gene 5 (*Irx5*), POU domain class 4 transcription factor 1 (*Pouf4f1*) and LIM homeobox 9 (*Lhx9*) (Cheng et al., 2005; Danno et al., 2008; Gage et al., 2008; Badea and Nathans, 2011; Bharti et al., 2012; Balasubramanian et al., 2014). *Fgf15*, *Otx2* and *Lhx9* counts were increased more than twofold, *Pou4f1* expression showed a threefold increase, and *Irx5* and *Pitx2* counts were elevated almost by a factor of four in *Sox2-creER^{T2}::Brg1$^{fl/fl}$::lslRFP$^{fl/fl}$*- compared with *Sox2-creER^{T2}::lslRFP$^{fl/fl}$*-derived cells.

Increased FGF signaling induces transdifferentiation of RPE cells to NR *in vitro* (Zhao et al., 1995). Furthermore, in a mouse model investigating RPE development, *Fgf15* was specifically upregulated upon RPE to NR transdifferentiation (Bharti et al., 2012). As we isolated RFP-positive cells from the entire E14.5 brain, including the enlarged NR attached to the basal cerebrum, we hypothesize that the mutant NR was the result of a RPE to NR transdifferentiation caused by increased FGF signaling. The RPE is a single layer of cells adjacent to the outer layers of the NR (Fig. 6B). In *Sox2-creER^{T2}::Brg1$^{fl/fl}$* mice with *Brg1* deletion at E7.5, the RPE was visible only in some regions (Fig. 6D) and seemed to transition into NR (white arrow), supporting the hypothesis of a transdifferentiation. BRG1-negative cells were predominantly found outside the enlarged NR in locations where the RPE is normally present (Fig. 6C,E, blue arrows). Furthermore, we found single pigmented cells close to BRG1-negative cells (Fig. 6E, blue arrowheads), indicating that BRG1 loss in the RPE might cause transdifferentiation into NR.

In order to validate whether the RPE was derived from those cells, in which we had activated the Cre recombinase at E7.5, we examined the RFP signal in the previously used fate-mapping mice (Fig. 5A). RFP-positive cells were found in the brain, the NR and the RPE at E18.5 (Fig. S7). By confirming that the RPE was also affected by the Cre-mediated recombination using the fate-mapping approach, we further support the hypothesis that the enlarged NR might result from a RPE to NR transdifferentiation.

As we suspected that increased FGF15 signaling was responsible for the formation of the enlarged NR, we performed IF demonstrating that the mutant NR expressed high amounts of FGF15 protein (Fig. 6I). Additionally, alterations in the mitogen-activated protein kinase (MAPK) signaling pathway as a potential consequence of increased FGF15 signaling were present (Fig. S8A). Phosphorylated ERK 1,2 (p-ERK 1,2) showed no activity in the NR of healthy controls (Fig. S8B) but displayed patchy reactivity in the enlarged NR (Fig. S8C). Likewise, we found changes in the MAPK signaling pathways after loss of *Brg1* at E9.5 (Fig. S8A) accompanied by a high reactivity for p-ERK 1,2 in the rosette-like structures of the SVZ (Fig. S8E). This indicates that *Brg1* plays a general role in the regulation of MAPK signaling.

To further support the hypothesis that the altered NR was the result of a transdifferentiation of RPE to NR, we stained for ezrin, a marker for the microvilli of the RPE (Bonilha et al., 2006) (Fig. 6G,J). Ezrin identified normal appearing RPE (Fig. 6J, green arrow), and Ezrin expression was also detectable in cells arranged in multiple layers (green arrowhead). Finally, we stained for NR2F1 (Coup-TFI), which is essential for proper eye development (Tang et al., 2010), and determined that the enlarged NR in *Sox2-creER^{T2}::Brg1$^{fl/fl}$* mice (Fig. 6K) had a similar NR2F1 expression pattern to the NR of E11.5 mice (Tang et al., 2010), suggesting that it was more immature than its E18.5 counterpart (Fig. 6H).

Based on these results, we hypothesized that *Brg1* loss at E7.5 in *Sox2*-expressing cells resulted in the dysregulation of genes that are essential for normal eye development. Consequently, the RPE, at least parts of it, did not develop normally but instead gave rise to an immature NR.

Development (2021) 148, dev196147. doi:10.1242/dev.196147

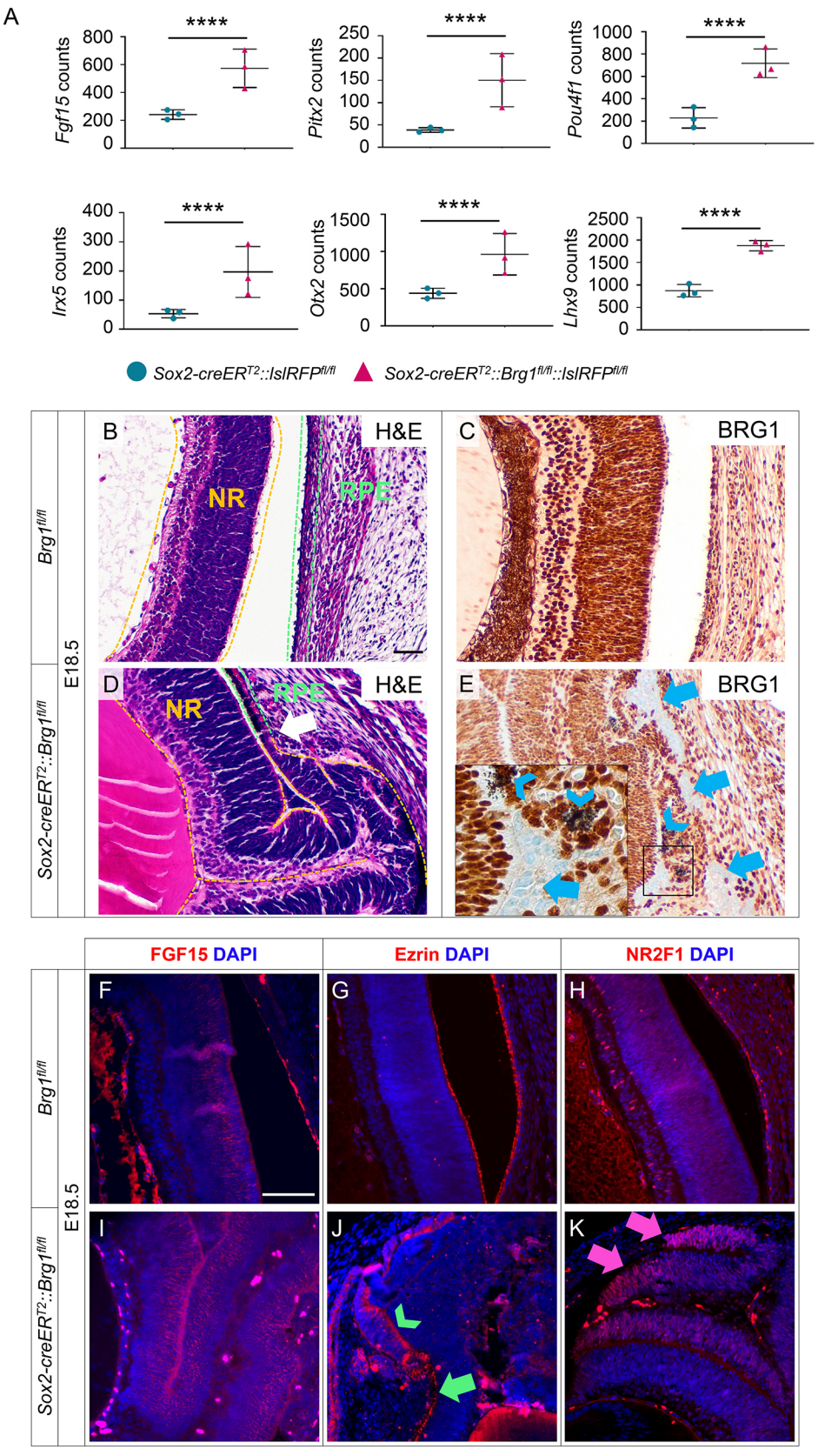

Fig. 6. *Brg1* deficiency induces transdifferentiation of retinal pigment epithelium into neural retina. (A) *Brg1* deletion at E7.5 leads to the upregulation of *Fgf15*, *Pitx2*, *Irx5*, *Pou4f1*, *Otx2* and *Lhx9* in RFP-expressing cells isolated at E14.5 from *Sox2-creER^{T2}::Brg1$^{fl/fl}$::RFP$^{fl/fl}$* embryos. Data are mean±s.d. ****P<0.0001. (B,D) Neural retina (NR) and retinal pigment epithelium (RPE) in a healthy control (B) and in a representative *Sox2-creER^{T2}::Brg1$^{fl/fl}$* embryo (D) at E18.5 are marked in orange and green, respectively. The white arrow indicates a region of transition of retained RPE into NR. (C,E) BRG1 is expressed in all cells of the eye in controls (C) but lost in a fraction of cells in mutants (E). BRG1-negative cells are highlighted with a blue arrow and pigmented cells with a blue arrowhead. Images were taken in a 100× magnification. (F-K) FGF15, Ezrin and NR2F1 protein are shown in sections of *Brg1$^{fl/fl}$* (F-H) and *Sox2-creER^{T2}::Brg1$^{fl/fl}$::RFP$^{fl/fl}$* (I-K) eyes at a 400× magnification. The green arrow shows retained RPE and the green arrowhead shows Ezrin-expressing cells that are morphologically distinct from normal RPE cells. The pink arrows indicate NR2F1-expressing cells in the enlarged NR. All images were taken from E18.5 embryos. n≥3 animals. Scale bars: 50 µm in B-E; 100 µm in F-K.

DISCUSSION

The presence of *BRG1* mutations in several different human diseases suggests a context-dependent role of this gene (Hasselblatt et al., 2014; Lang and Hendricks, 2018; Sekiguchi et al., 2019). Furthermore, different mouse models indicate that *Brg1* is essential for several steps of brain ontogenesis (Lessard et al., 2007; Matsumoto et al., 2016). Here, we investigated how an early *Brg1* loss in NSCs affected neural development. Furthermore,

Development (2021) 148, dev196147. doi:10.1242/dev.196147

we examined whether *Brg1* has time-specific roles and deleted the protein at different time points during embryonic development. *Sox2* is the first intrinsic marker for neural identity during development (Adnani et al., 2018). We therefore used *Sox2-creER^{T2}* mice to induce *Brg1* deficiency between E6.5 and E14.5.

Brg1 deficiency altered embryonic brain development only when it was induced between E7.5 and E12.5, but not at E6.5 or E14.5. The deletion between E7.5 and E12.5 caused diverse and time point-dependent architectural abnormalities in the brains and eyes of *Sox2-creER^{T2}::Brg1$^{fl/fl}$* embryos. Exclusively at E7.5 and E8.5, *Brg1* loss caused the formation of an enlarged NR. Between E8.5 and E10.5, *Brg1* deprivation led to alterations in the neocortex in a fraction of animals. In contrast, the architecture of the SVZ was affected in the majority of animals irrespective of the time of tamoxifen-induced *Brg1* deficiency and was also observed in *Sox2-creER^{T2}::Ini1$^{fl/fl}$* embryos after an *Ini1* loss induced at E9.5. These observations suggest that the NSCs of the SVZ are particularly sensitive towards alterations in the SWI/SNF complex at E9.5. However, the phenotypes outside the SVZ observed between E7.5 and E12.5 in *Sox2-creER^{T2}::Brg1$^{fl/fl}$* embryos imply *Brg1*-specific roles in eye and brain development.

As the SVZ is one of the germinal zones harboring mainly NSCs, it seemed likely that this region was highly affected by the NSC-specific loss of *Brg1*. Unexpectedly, the SVZ, including the rosette-like structures, was mainly composed of BRG1-positive cells and BRG1-deficient cells were found only occasionally. This might be explained by the fact that cells essential for the integrity of the SVZ, e.g. by providing exocrine signals, were lacking. Analysis of pHH3 and clCasp3 expression 3 days after *Brg1* loss at E7.5 revealed no changes in proliferation but an increase in apoptotic cells. Concordantly, using a fate-mapping approach, we show that, upon deletion of *Brg1* at either E7.5 or E9.5, less BRG1-negative cells are found at E14.5. Furthermore, results from our neurosphere assay imply that *Brg1*-deprived NSCs are unable to survive and proliferate *in vitro*. Previous studies have already demonstrated that *Brg1* knockdown can result in enhanced apoptosis (Deng et al., 2015; Singh et al., 2016). Therefore, we hypothesize that *Brg1* loss causes an increase in apoptosis, causing a lack of precursor cells in the SVZ.

We also identified changes in gene expression responsible for the observed morphological alterations. Therefore, we did not only observe distinct changes in gene expression between *Brg1*-negative and *Brg1*-competent cells but also between cells with *Brg1* loss induced either at E7.5 or at E9.5. Based on these data, we conclude that *Brg1* facilitates important functions regulating transcription in *Sox2*-expressing NSCs. In addition, these data further support the hypothesis that the ATPase has distinct roles at different stages during early neural development. Enrichment analysis of GO terms revealed that GO terms specifically related to neuronal functions were downregulated after *Brg1* loss at E7.5 or E9.5. In particular, the functionality of synaptic cell-cell interactions seemed to be disturbed upon ablation of *Brg1* expression. As the morphology of the pyramidal neurons in the cortices of *hGFAP-cre::Brg1$^{fl/fl}$* mice was severely altered, we hypothesized that *Brg1* is not only important in murine NSCs marked by *hGFAP* (Holdhof et al., 2020) and in *Xenopus laevis* neurogenesis (Seo et al., 2005), but also in *Sox2*-expressing murine NSCs in order to give rise to functional neurons. Furthermore, disturbances in synaptic communication due to *Brg1* deficiency might explain the lack of BRG1-negative cells in the brain regions with morphological abnormalities. We hypothesize that *Brg1*-deficient cells transmit pathological signals to their neighboring (*Brg1*-competent) cells, causing the observed architectural alterations in a paracrine manner.

In addition, enrichment analysis of upregulated GO terms revealed the enhancement of terms related to the ECM, especially after *Brg1* loss at E9.5. As the ECM contributes to maintaining stem cell identity, e.g. by providing a reservoir of growth factors, BMPs or TGFβ, the alterations in ECM-related terms might be another cause for the disrupted SVZ (Barros et al., 2011; Brizzi et al., 2012). We recognized that the expression of collagen-encoding genes was upregulated upon *Brg1* loss at either E7.5 or E9.5. Notably, induction of *Brg1* deficiency at E9.5 additionally resulted in enhanced expression of other ECM-associated genes, many of which are found in fractones, a basement membrane-resembling structure found exclusively in the SVZ (Mercier et al., 2002; Kerever et al., 2007; Mercier, 2016). Even though fractones have only been described in the adult SVZ so far, to our knowledge, there is no evidence that they are not already present in the embryonic SVZ. They provide NSCs with growth factors, supporting their stem cell function. Therefore, a misbalance in the expression of fractone-associated genes might interfere with facilitating these functions. To sum up, the dysregulation of ECM-associated genes might also contribute to the SVZ phenotype observed in *Sox2-creER^{T2}::Brg1$^{fl/fl}$* embryos, especially when *Brg1* deficiency was induced at E9.5. Furthermore, the ECM also facilitates important functions in NSC differentiation, neuronal migration, the formation of axonal tracts, and the maturation and function of synapses (Barros et al., 2011). Therefore, the upregulation of ECM-associated genes and GO terms might also have an impact on these processes.

Of note, *Brg1* loss at E7.5 resulted in more downregulated GO terms related to neuronal functions, whereas *Brg1* deprivation at E9.5 instead caused the enhancement of GO terms, including those involved in ECM composition. In addition to the differences we observed in histology, this further highlights the time-specific role of *Brg1*. Still, as we observed a reduced efficiency of the Cre recombinase in *Sox2-creER^{T2}::Brg1$^{fl/fl}$::lslRFP$^{fl/fl}$* mice, we cannot rule out the possibility that we might have missed some DEGs contributing to the observed phenotypes.

In the developing cerebral cortex of *Sox2-creER^{T2}::Brg1$^{fl/fl}$* embryos, BRG1-deficient cells were scattered randomly across all layers. However, only in a fraction of embryos, *Brg1* deprivation resulted in disrupted layering in the deeper layers (VZ/SVZ) – the site that harbors neural progenitors. Maturation of neural progenitors into neurons is accompanied by a switch in the composition of the SWI/SNF complex. This contributes to distinct changes in gene expression needed for correct differentiation and migration of neurons during cortical development (Narayanan and Tuoc, 2014; Son and Crabtree, 2014; Elsen et al., 2018; Sokpor et al., 2018). However, as only the regions where neural progenitors reside were affected in *Sox2-creER^{T2}::Brg1$^{fl/fl}$* embryos, this phenotype might not reflect issues in cortical development. It is rather another example that the knockout of *Brg1* caused disruption of the NSC niche, as already discussed for the SVZ.

One of the most striking phenotypes in the *Sox2-creER^{T2}::Brg1$^{fl/fl}$* embryos was the enlarged mutant NR. It exclusively occurred after *Brg1* loss between E7.5 and E8.5, and was first detectable at E16.5. The overall morphology as well as the expression patterns of marker proteins was very similar to the physiological NR of healthy littermates. Transcriptome analysis revealed that genes that are expressed during normal eye development were upregulated upon *Brg1* loss at E7.5. *Pouf41*, for example, was one of the DEGs with the highest log2 fold change and is physiologically expressed in the embryonic NR from E12.5

Development (2021) 148, dev196147. doi:10.1242/dev.196147

onwards (Pan et al., 2005). Strikingly, *Fgf15* expression was also significantly upregulated upon *Brg1* loss at E7.5, and the enlarged NR showed high immunoreactivity for the FGF15 protein. In another mouse model, *Fgf15* transcription was enhanced in case of RPE to NR transdifferentiation (Bharti et al., 2012). Therefore, we hypothesized that the enlarged NR was also formed as a consequence of RPE to NR transdifferentiation in our model. The results of the fate-mapping experiment revealed that both NR and RPE harbor progenies of cells, in which we had activated Cre at E7.5. In addition, presumptive NR and RPE express Sox2 (Smith et al., 2009). Consequently, we cannot rule out the possibility that the enlarged NR is (partially) the result of uncontrolled proliferative activity of the NR itself. However, as we visually observed regions in which the RPE directly transitioned into the NR, it is more likely that loss of *Brg1* causes a transdifferentiation of the RPE into NR, and that *Brg1* plays an essential role in the maintenance of the proper RPE.

During eye development, RPE and NR originate from the same precursors and fate is determined by several extrinsic and intrinsic factors (Fuhrmann, 2010). Balance of these factors is crucial for proper eye development, as demonstrated by several mouse models, in which dysregulation of genes, such as *Mitf*, β-Catenin, transcription factor AP-2α or Yes-associated protein (*Yap*), resulted in RPE to NR transdifferentiation (West-Mays et al., 1999; Bumsted and Barnstable, 2000; Fujimura et al., 2009; Kim et al., 2016). So far, *Brg1* has not been associated with this process. However, the interaction of BRG1 itself or the SWI/SNF complex with many of the before-mentioned genes has already been reported (Laurette et al., 2015; Zhu et al., 2015; Chang et al., 2018). Additionally, *Brg1* has been described to be involved in retinogenesis (Aldiri et al., 2015). Finally, we occasionally detected rosette-like structures in the retina of *Sox2-creER^{T2}::Brg1$^{fl/fl}$* embryos with *Brg1* loss at E9.5. This indicates that, similar to the situation in the SVZ, certain cells that had lost *Brg1* earlier in development died, which in turn disrupts cell-cell interactions and causes the formation of rosettes. In line with these findings, *Brg1* has been described to be essential for eye development in zebrafish. There, a *Brg1* null mutation results in a NR without proper lamination and in disruption during the differentiation of retinal cells (Gregg et al., 2003). Finally, individuals with Coffin-Siris syndrome carrying *BRG1* germline mutations occasionally present with ophthalmological anomalies, including microphthalmia, strabismus or retinal dystrophy (Kosho et al., 2013; Errichiello et al., 2017; Cappuccio et al., 2019). As we did not observe any regions resembling enlarged NR in *Sox2-creER^{T2}::Ini1$^{fl/fl}$* mice, we assume that BRG1 and not the SWI/SNF complex as a whole is essential for repressing retinal fate. However, the temporal window seems very narrow, as we did not observe RPE-to-NR transdifferentiation when *Brg1* loss was induced earlier than E7.5 or later than E8.5.

In conclusion, proper expression of *Brg1* and *Ini1* in NSCs is essential for the integrity of the SVZ. In addition, *Brg1* is also essential for normal cortical development and maintenance of the RPE. As BRG1 is part of the SWI/SNF complex that regulates gene expression, these phenotypes are caused by dysregulation of cell type- and time-specific transcription.

MATERIALS AND METHODS

Mice

Brg1$^{fl/fl}$, *Ini1$^{fl/fl}$* (JAX #004596), *lslRFP$^{fl/fl}$* and *Sox2-creER^{T2}* (JAX #17593) mice have previously been generated and described (Sumi-Ichinose et al., 1997; Roberts et al., 2002; Indra et al., 2005; Luche et al., 2007; Arnold et al., 2011). They were crossed to generate *Sox2-creER^{T2}::Brg1$^{fl/fl}$*, *Sox2-creER^{T2}::Ini1$^{fl/fl}$*, *Sox2-creER^{T2}::lslRFP$^{fl/fl}$*, *Brg1$^{fl/fl}$::lslRFP$^{fl/fl}$* and *Sox2-creER^{T2}::Brg1$^{fl/fl}$::lslRFP$^{fl/fl}$* mice. Female *Brg1$^{fl/fl}$*, *Ini1$^{fl/fl}$*, *lslRFP$^{fl/fl}$* and *Brg1$^{fl/fl}$::lslRFP$^{fl/fl}$* mice were bred with male *Sox2-creER^{T2}::Brg1$^{fl/fl}$*, *Sox2-creER^{T2}::Ini1$^{fl/fl}$*, *Sox2-creER^{T2}::lslRFP$^{fl/fl}$* and *Sox2-creER^{T2}::Brg1$^{fl/fl}$::lslRFP$^{fl/fl}$* mice. A single dose of 1 mg tamoxifen in 50 µl corn oil was injected intraperitoneally into pregnant mice at E6.5, E7.5, E8.5, E9.5, E10.5, E12.5 or E14.5 to induce Cre recombinase activity. The observation of a post-coital plug was defined as E0.5. The fate-mapping mice were generated for better characterization of *Brg1*-deficient cell populations: mothers of *Sox2-creER^{T2}::lslRFP$^{fl/fl}$* (controls) and *Sox2-creER^{T2}::Brg1$^{fl/fl}$::lslRFP$^{fl/fl}$* (mutants) received tamoxifen at either E7.5 or E9.5. Embryos were collected by Caesarean section. Ear or tail biopsies were used for genotyping via PCR. The following primers were used to detect the *cre* transgene (448 bp), the *Brg1* wild type (241 bp) or floxed (387 bp) allele, the *Ini1* wild type (203 bp) or floxed (300 bp) allele and the *lslRFP* wild type (600 bp) or mutant (250 bp) allele: 5′-TCCGGG-CTGCCACGACCAA-3′ (*cre* forward), 5′-GGCGCGGCAACACCATT-TT-3′ (*cre* reverse), 5′-GTCATACTTATGTCATAGCC-3′ (*Brg1* forward), 5′-GCCTTGTCTCAAACTGATAAG-3′ (*Brg1* reverse), 5′-TAGGCAC-TGGACATAAGGGC-3′ (*Ini1* forward), 5′-GTAACTGTCAAGAATCAA-TGG-3′ (*Ini1* reverse), 5′-AAAGTCGCTCTGAGTTGTTAT-3′ (*lslRFP* forward), 5′-GCGAAGAGTTTGTCCTCAACC-3′ (*lslRFP* mutant reverse) and 5′-GGAGCGGGAGAAATGGATATG-3′ (*lslRFP* wild-type reverse). Mice were kept on a 12 h dark/light cycle and water and food was available *ad libitum*. Animals of both sexes were used for the experiments. The mice belonged to the species *Mus musculus* and were maintained on a C57Bl/6J background. The experimental procedures were approved by the Government of Hamburg, Germany (113/16, 19N099/2019) and the Government of Nordrhein-Westfalen, Germany (84-02.04.2015.A088).

Hematoxylin and Eosin staining, and immunohistochemistry

For Hematoxylin and Eosin as well as immunohistochemical stains, entire embryo heads (E12.5-E18.5) or whole embryos (E10.5) were fixed in 4% formaldehyde for 24 h. Afterwards, they were dehydrated, embedded in paraffin in a frontal orientation and 4 µm sections were cut according to established protocols. Hematoxylin and Eosin stains were performed according to standard protocols. Immunohistochemical stains were prepared using the Ventana System (Roche Diagnostics) or the DCS SuperVision 2 Kit (DCS Diagnostics) according to the manufacturers' instructions. The following antibodies were used: rabbit anti-Brg1 (Abcam, ab110641, 1:25), rabbit anti-cleaved caspase 3 (cl. Casp3; Asp175; Cell Signaling, #9664, 1:100), mouse anti-Ini1 (BD Biosciences, 1:50), mouse anti-phospho-Histone H3 (pHH3, Cell Signaling, #9706, 1:200), rabbit anti-Ki67 (Abcam, ab15580, 1:100), rabbit anti-Olig2 (Millipore, AB9610, 1:200), mouse anti-Otx2 (ThermoFisher Scientific, 1H12C4B5, 1:2000), rabbit anti-Pax6 (Biolegend, 901301, 1:1000), rabbit anti-Sox2 (Abcam, ab97959, 1:200) and mouse anti-TuJ1 (Biolegend, 801201,1:200). For all images, at least n=3 embryos were analyzed.

Immunofluorescent staining of paraffin wax-embedded or frozen tissue

For immunofluorescence, entire embryo heads were fixed in 4% formaldehyde for 24 h and processed according to standard protocols. For the detection of Ezrin, FGF15, NR2F1, phosphorylated ERK1/2 (p-ERK1/2) or phosphorylated SMAD1/5/8 (p-SMAD1/5/8), heads were dehydrated, embedded in paraffin wax in a frontal orientation and cut into 4 µm sections. Antigen retrieval was achieved by cooking the slides in citrate buffer (Ezrin, NR2F1 and p-SMAD1/5/8) or Tris-EDTA (FGF15 and p-ERK1/2) for 20 min. For the detection of RFP, the tissue was sequentially placed in 10%, 20% and 30% sucrose in PBS, and then placed into optimal cutting temperature compound (OCT, Sakura, #4583) in a frontal orientation. The following antibodies were used: mouse anti-Ezrin (Abcam, ab4069, 1:100), mouse anti-FGF15 (Santa Cruz, sc-514647, 1:50), mouse anti-NR2F1 (R&D system, PP-H8312-00, 1:100), rabbit anti-p-ERK1/2 (Cell Signaling, #4370, 1:100), rabbit anti-p-SMAD1/5/8 (Merck, AB3848-I, 1:50), rabbit anti-RFP (Novus Biologicals, NBP2-25157, 1:250), goat anti-mouse Alexa Fluor 555 (Cell Signaling, CST4409S, 1:500) and goat anti-rabbit Alexa Fluor 488 (Cell Signaling, CST4412S, 1:500). Nuclei were counterstained with DAPI (Roth, 1:1000 from a 1 mg/ml stock solution).

Development (2021) 148, dev196147. doi:10.1242/dev.196147

Fluorescence-activated cell sorting

Fate-mapping mice (*Sox2-creER^{T2}::lslRFP$^{fl/fl}$* and *Sox2-creER^{T2}::Brg1$^{fl/fl}$::lslRFP$^{fl/fl}$* mice after tamoxifen at E7.5 or E9.5) were sacrificed at E14.5 and their brains isolated under a dissecting microscope. The meninges were removed and the tissue digested using Papain (20 U/ml) and DNase (400 µg/ml) for 30 min at 37°C. RFP-positive cells were sorted using the BD FACS Aria-Fusion and the software FACSDiva 8.0.1 (both BD Biosciences).

Cytospin

After FACS, 5×10^5 RFP-positive cells were collected in 80 µl PBS and centrifuged for 5 min at 165 ***g*** onto a cytoslide using a cytospin centrifuge (Cytospin 4, Thermo Fisher Scientific). The cells were fixed with 4% formaldehyde for 20 min and air-dried overnight.

Immunofluorescence of fixed cells

Immunofluorescent staining was performed according to standard protocols and by using rabbit anti-Brg1 (Abcam, ab110641, 1:25) and goat anti-rabbit Alexa Fluor 488 (Cell Signaling, CST4412S, 1:500) antibodies. Nuclei were counterstained with DAPI (Roth, 1:1000 from a 1 mg/ml stock solution).

Neurosphere assay

RFP-positive cells collected by FACS were seeded in 500 µl culture medium [DMEM/F12 supplemented with 1 M HEPES buffer, N2 supplement, L-Glutamin, penicillin/streptomycin (50 U/ml), non-essential amino acids, epidermal growth factor (EGF, 20 ng/ml) and FGF (10 ng/ml)] at a concentration of 50 cells/µl. Every 3 days, fresh EGF and FGF were added to the medium. After 7 days in culture, number and size of primary neurospheres were determined using a Nikon Ti2 microscope (Nikon, Tokyo, JP) and quantified using the ImageJ software.

Statistics

All statistical tests were performed using the Prism Software Version 7 (GraphPad Software). Fractions of cell counts were blindly determined by counting the total number of cells per field (identified by staining of Hematoxylin) and the number of cells that stained positive for the respective marker (pHH3 or clCasp3). Statistical significance was determined by unpaired two-tailed *t*-tests. The yield of RFP-positive cells after FACS as well as the numbers of neurospheres per well after 7 days *in vitro* was compared by unpaired two-tailed *t*-tests.

RNA-sequencing

Total RNA of RFP-positive cells collected by FACS was isolated using TRIzol (Life Technologies) according to established protocols (Chomczynski, 1993). After isolation, the RNA integrity was analyzed with the RNA 6000 Nano Chip on an Agilent 2100 Bioanalyzer (Agilent Technologies). From total RNA, mRNA was extracted using the NEBNext Poly(A) mRNA Magnetic Isolation module (New England Biolabs) and RNA-Seq libraries were generated using the NEXTFLEX Rapid Directional qRNA-Seq Kit (Bioo Scientific) according to the manufacturer's recommendations. Concentrations of all samples were measured with a Qubit 2.0 Fluorometer (Thermo Fisher Scientific) and fragment lengths distribution of the final libraries was analyzed with the DNA High Sensitivity Chip on an Agilent 2100 Bioanalyzer (Agilent Technologies). All samples were normalized to 2 nM and pooled equimolarily. The library pool was sequenced on the NextSeq500 (Illumina) with 1×75 bp, with 14.2 to 19.7 mio reads per sample.

RNA-sequencing data analysis

The quality of the raw reads was confirmed by using the FastQC tool from the Babraham Bioinformatics Institute (Cambridge, UK). Afterwards, the reads were aligned to the mouse reference genome GRCm38 employing the Spliced Transcripts Alignment to a Reference (STAR) software (v.2.6.1c) (Dobin et al., 2013). Concurrently, counts (reads/gene) were determined by the quantmode GeneCounts option. They are based on the Ensembl annotation release 95 (Yates et al., 2020). The DESeq2 package (v.1.22.2) was used to estimate DEGs between *Brg1*-deficient samples and their *Brg1*-competent controls (Love et al., 2014). The package calculated log2 fold changes, *p*-values and FDRs. Genes were defined as DEGs, if they had a log2 fold change >±0.6 and a FDR <0.1. Heatmaps were created with the pheatmap R package, based on the DEseq2 normalized counts. Enriched GO terms were estimated with the GAGE R package (v2.32.1). To visualize GO terms and their related DEGs, GOchords were created by using the GOChord plotting function of the R package GOplot (v1.0.2). For KEGG Pathway analysis and visualization, R packages gage (v2.36.0) (Luo et al., 2009) and ReactomePA (v1.30.0) (Yu and He, 2016) were employed.

Acknowledgements

We thank Margarethe Gregersen, Kristin Hartmann, Vanessa Thaden, Jacqueline Kolanski, Anne Reichstein, Nick Mohr, Celina Soltwedel (all University Medical Center Hamburg-Eppendorf), Arne Düsedau, Jana Hennesen and Gundula Pilnitz-Stolze (all Leibniz Institute for Experimental Virology, Hamburg) for excellent technical support. We further thank Dr Pierre Chambon (IGBMC, Illkirch-Graffenstaden, France) for providing the *Brg1$^{fl/fl}$* mice. Finally, we acknowledge the support of the Small animal models core facility of the Heinrich Pette Institute. The data presented here were collected as part of the PhD thesis of D.H. (Holdhof, 2020).

Competing interests

The authors declare no competing or financial interests.

Author contributions

Conceptualization: D.H., U.S.; Methodology: D.H., M. Schoof, M. Spohn, C.K., C.G., M.H., D.I., N.M.; Software: M. Spohn; Formal analysis: D.H., M. Spohn; Investigation: D.H., S.A.; Resources: K.K., U.S.; Writing - original draft: D.H.; Writing - review & editing: D.H., M. Schoof, M. Spohn, D.I., N.M., K.K., U.S.; Visualization: D.H., S.A.; Supervision: U.S.; Project administration: U.S.; Funding acquisition: U.S.

Funding

This work was supported by the Deutsche Krebshilfe and the Wilhelm Sander Stiftung. U.S. was additionally supported by the Fördergemeinschaft Kinderkrebszentrum Hamburg.

Data availability

RNA-seq data may be obtained from European Nucleotide Archive (ENA) under accession number PRJEB39755.

Peer review history

The peer review history is available online at https://journals.biologists.com/dev/article-lookup/doi/10.1242/dev.196147

References

Adnani, L., Han, S., Li, S., Mattar, P. and Schuurmans, C. (2018). Mechanisms of cortical differentiation. *Int. Rev. Cell Mol. Biol.* **336**, 223-320. doi:10.1016/bs.ircmb.2017.07.005

Aldiri, I., Ajioka, I., Xu, B., Zhang, J., Chen, X., Benavente, C., Finkelstein, D., Johnson, D., Akiyama, J., Pennacchio, L. A. et al. (2015). Brg1 coordinates multiple processes during retinogenesis and is a tumor suppressor in retinoblastoma. *Development* **142**, 4092-4106. doi:10.1242/dev.124800

Alpsoy, A. and Dykhuizen, E. C. (2018). Glioma tumor suppressor candidate region gene 1 (GLTSCR1) and its paralog GLTSCR1-like form SWI/SNF chromatin remodeling subcomplexes. *J. Biol. Chem.* **293**, 3892-3903. doi:10.1074/jbc.RA117.001065

Arnold, K., Sarkar, A., Yram, M. A., Polo, J. M., Bronson, R., Sengupta, S., Seandel, M., Geijsen, N. and Hochedlinger, K. (2011). Sox2(+) adult stem and progenitor cells are important for tissue regeneration and survival of mice. *Cell Stem Cell* **9**, 317-329. doi:10.1016/j.stem.2011.09.001

Badea, T. C. and Nathans, J. (2011). Morphologies of mouse retinal ganglion cells expressing transcription factors Brn3a, Brn3b, and Brn3c: analysis of wild type and mutant cells using genetically-directed sparse labeling. *Vision Res.* **51**, 269-279. doi:10.1016/j.visres.2010.08.039

Balasubramanian, R., Bui, A., Ding, Q. and Gan, L. (2014). Expression of LIM-homeodomain transcription factors in the developing and mature mouse retina. *Gene Expr. Patterns* **14**, 1-8. doi:10.1016/j.gep.2013.12.001

Barros, C. S., Franco, S. J. and Müller, U. (2011). Extracellular matrix: functions in the nervous system. *Cold Spring Harb. Perspect Biol.* **3**, a005108. doi:10.1101/cshperspect.a005108

Belkin, A. M. and Stepp, M. A. (2000). Integrins as receptors for laminins. *Microsc. Res. Tech.* **51**, 280-301. doi:10.1002/1097-0029(20001101)51:3<280::AID-JEMT7>3.0.CO;2-O

Bharti, K., Gasper, M., Ou, J., Brucato, M., Clore-Gronenborn, K., Pickel, J. and Arnheiter, H. (2012). A regulatory loop involving PAX6, MITF, and WNT signaling controls retinal pigment epithelium development. *PLoS Genet.* **8**, e1002757. doi:10.1371/journal.pgen.1002757

Bischof, M., Weider, M., Kuspert, M., Nave, K.-A. and Wegner, M. (2015). Brg1-dependent chromatin remodelling is not essentially required during oligodendroglial differentiation. *J. Neurosci.* **35**, 21-35. doi:10.1523/JNEUROSCI.1468-14.2015

Bonilha, V. L., Rayborn, M. E., Saotome, I., McClatchey, A. I. and Hollyfield, J. G. (2006). Microvilli defects in retinas of ezrin knockout mice. *Exp. Eye Res.* **82**, 720-729. doi:10.1016/j.exer.2005.09.013

Brizzi, M. F., Tarone, G. and Defilippi, P. (2012). Extracellular matrix, integrins, and growth factors as tailors of the stem cell niche. *Curr. Opin. Cell Biol.* **24**, 645-651. doi:10.1016/j.ceb.2012.07.001

Bultman, S., Gebuhr, T., Yee, D., La Mantia, C., Nicholson, J., Gilliam, A., Randazzo, F., Metzger, D., Chambon, P., Crabtree, G. et al. (2000). A Brg1 null mutation in the mouse reveals functional differences among mammalian SWI/SNF complexes. *Mol. Cell* **6**, 1287-1295. doi:10.1016/S1097-2765(00)00127-1

Bultman, S. J., Herschkowitz, J. I., Godfrey, V., Gebuhr, T. C., Yaniv, M., Perou, C. M. and Magnuson, T. (2008). Characterization of mammary tumors from Brg1 heterozygous mice. *Oncogene* **27**, 460-468. doi:10.1038/sj.onc.1210664

Bumsted, K. M. and Barnstable, C. J. (2000). Dorsal retinal pigment epithelium differentiates as neural retina in the microphthalmia (mi/mi) mouse. *Invest. Ophthalmol. Vis. Sci.* **41**, 903-908.

Cappuccio, G., Brunetti-Pierri, R., Torella, A., Pinelli, M., Castello, R., Casari, G., Nigro, V., Banfi, S., Simonelli, F. and Brunetti-Pierri, N. (2019). Retinal dystrophy in an individual carrying a de novo missense variant of SMARCA4. *Mol. Genet Genomic Med.* **7**, e682. doi:10.1002/mgg3.682

Chang, L., Azzolin, L., Di Biagio, D., Zanconato, F., Battilana, G., Lucon Xiccato, R., Aragona, M., Giulitti, S., Panciera, T., Gandin, A. et al. (2018). The SWI/SNF complex is a mechanoregulated inhibitor of YAP and TAZ. *Nature* **563**, 265-269. doi:10.1038/s41586-018-0658-1

Chen, V. S., Morrison, J. P., Southwell, M. F., Foley, J. F., Bolon, B. and Elmore, S. A. (2017). Histology atlas of the developing prenatal and postnatal mouse central nervous system, with emphasis on prenatal days E7.5 to E18.5. *Toxicol. Pathol.* **45**, 705-744. doi:10.1177/0192623317728134

Cheng, C. W., Chow, R. L., Lebel, M., Sakuma, R., Cheung, H. O., Thanabalasingham, V., Zhang, X., Bruneau, B. G., Birch, D. G., Hui, C. C. et al. (2005). The Iroquois homeobox gene, Irx5, is required for retinal cone bipolar cell development. *Dev. Biol.* **287**, 48-60. doi:10.1016/j.ydbio.2005.08.029

Chiba, H., Muramatsu, M., Nomoto, A. and Kato, H. (1994). Two human homologues of Saccharomyces cerevisiae SWI2/SNF2 and Drosophila brahma are transcriptional coactivators cooperating with the estrogen receptor and the retinoic acid receptor. *Nucleic Acids Res.* **22**, 1815-1820. doi:10.1093/nar/22.10.1815

Chomczynski, P. (1993). A reagent for the single-step simultaneous isolation of RNA, DNA and proteins from cell and tissue samples. *Biotechniques* **15**, 532-534, 536-537.

Danno, H., Michiue, T., Hitachi, K., Yukita, A., Ishiura, S. and Asashima, M. (2008). Molecular links among the causative genes for ocular malformation: Otx2 and Sox2 coregulate Rax expression. *Proc. Natl. Acad. Sci. USA* **105**, 5408-5413. doi:10.1073/pnas.0710954105

De Rubeis, S., He, X., Goldberg, A. P., Poultney, C. S., Samocha, K., Cicek, A. E., Kou, Y., Liu, L., Fromer, M., Walker, S. et al. (2014). Synaptic, transcriptional and chromatin genes disrupted in autism. *Nature* **515**, 209-215. doi:10.1038/nature13772

Deng, L., Li, G., Rao, B. and Li, H. (2015). Central nervous system-specific knockout of Brg1 causes growth retardation and neuronal degeneration. *Brain Res.* **1622**, 186-195. doi:10.1016/j.brainres.2015.06.027

Dobin, A., Davis, C. A., Schlesinger, F., Drenkow, J., Zaleski, C., Jha, S., Batut, P., Chaisson, M. and Gingeras, T. R. (2013). STAR: ultrafast universal RNA-seq aligner. *Bioinformatics* **29**, 15-21. doi:10.1093/bioinformatics/bts635

Dutta, A., Sardiu, M., Gogol, M., Gilmore, J., Zhang, D., Florens, L., Abmayr, S. M., Washburn, M. P. and Workman, J. L. (2017). Composition and function of mutant Swi/Snf complexes. *Cell Rep* **18**, 2124-2134. doi:10.1016/j.celrep.2017.01.058

Elsen, G. E., Bedogni, F., Hodge, R. D., Bammler, T. K., MacDonald, J. W., Lindtner, S., Rubenstein, J. L. R. and Hevner, R. F. (2018). The epigenetic factor landscape of developing neocortex is regulated by transcription factors Pax6→ Tbr2→ Tbr1. *Front Neurosci,* **12**, 571. doi:10.3389/fnins.2018.00571

Errichiello, E., Mustafa, N., Vetro, A., Notarangelo, L. D., de Jonge, H., Rinaldi, B., Vergani, D., Giglio, S. R., Morbini, P. and Zuffardi, O. (2017). SMARCA4 inactivating mutations cause concomitant Coffin-Siris syndrome, microphthalmia and small-cell carcinoma of the ovary hypercalcaemic type. *J. Pathol.* **243**, 9-15. doi:10.1002/path.4926

Fuhrmann, S. (2010). Eye morphogenesis and patterning of the optic vesicle. *Curr Top Dev Biol,* **93**, 61-84. doi:10.1016/B978-0-12-385044-7.00003-5

Fujimura, N., Taketo, M. M., Mori, M., Korinek, V. and Kozmik, Z. (2009). Spatial and temporal regulation of Wnt/beta-catenin signaling is essential for development of the retinal pigment epithelium. *Dev. Biol.* **334**, 31-45. doi:10.1016/j.ydbio.2009.07.002

Gage, P. J., Qian, M., Wu, D. and Rosenberg, K. I. (2008). The canonical Wnt signaling antagonist DKK2 is an essential effector of PITX2 function during normal eye development. *Dev. Biol.* **317**, 310-324. doi:10.1016/j.ydbio.2008.02.030

Gregg, R. G., Willer, G. B., Fadool, J. M., Dowling, J. E. and Link, B. A. (2003). Positional cloning of the young mutation identifies an essential role for the Brahma chromatin remodeling complex in mediating retinal cell differentiation. *Proc. Natl. Acad. Sci. U.S.A.* **100**, 6535-6540. doi:10.1073/pnas.0631813100

Hargreaves, D. C. and Crabtree, G. R. (2011). ATP-dependent chromatin remodeling: genetics, genomics and mechanisms. *Cell Res.* **21**, 396-420. doi:10.1038/cr.2011.32

Hasselblatt, M., Nagel, I., Oyen, F., Bartelheim, K., Russell, R. B., Schüller, U., Junckerstorff, R., Rosenblum, M., Alassiri, A. H., Rossi, S. et al. (2014). SMARCA4-mutated atypical teratoid/rhabdoid tumors are associated with inherited germline alterations and poor prognosis. *Acta Neuropathol.* **128**, 453-456. doi:10.1007/s00401-014-1323-x

Ho, L., Ronan, J. L., Wu, J., Staahl, B. T., Chen, L., Kuo, A., Lessard, J., Nesvizhskii, A. I., Ranish, J. and Crabtree, G. R. (2009). An embryonic stem cell chromatin remodeling complex, esBAF, is essential for embryonic stem cell self-renewal and pluripotency. *Proc. Natl. Acad. Sci. U.S.A.* **106**, 5181-5186. doi:10.1073/pnas.0812889106

Holdhof, D. (2020). Brg1 in neural development and disease. *PhD Thesis*.

Holdhof, D., Schoof, M., Hellwig, M., Holdhof, N. H., Niesen, J. and Schüller, U. (2020). hGFAP-positive stem cells depend on Brg1 for proper formation of cerebral and cerebellar structures. *Cereb. Cortex* **30**, 1382-1392.

Holdhof, D., Johann, P. D., Spohn, M., Bockmayr, M., Safaei, S., Joshi, P., Masliah-Planchon, J., Ho, B., Andrianteranagna, M., Bourdeaut, F. et al. (2021). Atypical teratoid/rhabdoid tumors (ATRTs) with SMARCA4 mutation are molecularly distinct from SMARCB1-deficient cases. *Acta Neuropathol.* **141**, 291-301. doi:10.1007/s00401-020-02250-7

Holsten, T., Bens, S., Oyen, F., Nemes, K., Hasselblatt, M., Kordes, U., Siebert, R., Frühwald, M. C., Schneppenheim, R. and Schüller, U. (2018). Germline variants in SMARCB1 and other members of the BAF chromatin-remodeling complex across human disease entities: a meta-analysis. *Eur. J. Hum. Genet.* **26**, 1083-1093. doi:10.1038/s41431-018-0143-1

Indra, A. K., Dupe, V., Bornert, J. M., Messaddeq, N., Yaniv, M., Mark, M., Chambon, P. and Metzger, D. (2005). Temporally controlled targeted somatic mutagenesis in embryonic surface ectoderm and fetal epidermal keratinocytes unveils two distinct developmental functions of BRG1 in limb morphogenesis and skin barrier formation. *Development* **132**, 4533-4544. doi:10.1242/dev.02019

Kerever, A., Schnack, J., Vellinga, D., Ichikawa, N., Moon, C., Arikawa-Hirasawa, E., Efird, J. T. and Mercier, F. (2007). Novel extracellular matrix structures in the neural stem cell niche capture the neurogenic factor fibroblast growth factor 2 from the extracellular milieu. *Stem Cells* **25**, 2146-2157. doi:10.1634/stemcells.2007-0082

Kim, J. Y., Park, R., Lee, J. H., Shin, J., Nickas, J., Kim, S. and Cho, S. H. (2016). Yap is essential for retinal progenitor cell cycle progression and RPE cell fate acquisition in the developing mouse eye. *Dev. Biol.* **419**, 336-347. doi:10.1016/j.ydbio.2016.09.001

Kosho, T., Okamoto, N., Ohashi, H., Tsurusaki, Y., Imai, Y., Hibi-Ko, Y., Kawame, H., Homma, T., Tanabe, S., Kato, M. et al. (2013). Clinical correlations of mutations affecting six components of the SWI/SNF complex: detailed description of 21 patients and a review of the literature. *Am. J. Med. Genet. A* **161a**, 1221-1237. doi:10.1002/ajmg.a.35933

Kwon, H., Imbalzano, A. N., Khavari, P. A., Kingston, R. E. and Green, M. R. (1994). Nucleosome disruption and enhancement of activator binding by a human SW1/SNF complex. *Nature* **370**, 477-481. doi:10.1038/370477a0

Lang, J. D. and Hendricks, W. P. D. (2018). Identification of driver mutations in rare cancers: the role of SMARCA4 in small cell carcinoma of the ovary, hypercalcemic type (SCCOHT). *Methods Mol. Biol.* **1706**, 367-379. doi:10.1007/978-1-4939-7471-9_20

Laurette, P., Strub, T., Koludrovic, D., Keime, C., Le Gras, S., Seberg, H., Van Otterloo, E., Imrichova, H., Siddaway, R., Aerts, S. et al. (2015). Transcription factor MITF and remodeller BRG1 define chromatin organisation at regulatory elements in melanoma cells. *Elife* **4**, e06857. doi:10.7554/eLife.06857.025

Lessard, J., Wu, J. I., Ranish, J. A., Wan, M., Winslow, M. M., Staahl, B. T., Wu, H., Aebersold, R., Graef, I. A. and Crabtree, G. R. (2007). An essential switch in subunit composition of a chromatin remodeling complex during neural development. *Neuron* **55**, 201-215. doi:10.1016/j.neuron.2007.06.019

Li, D., Ahrens-Nicklas, R. C., Baker, J., Bhambhani, V., Calhoun, A., Cohen, J. S., Deardorff, M. A., Fernández-Jaén, A., Kamien, B., Jain, M. et al. (2020). The variability of SMARCA4-related Coffin-Siris syndrome: do nonsense candidate variants add to milder phenotypes? *Am. J. Med. Genet. A* **182**, 2058-2067. doi:10.1002/ajmg.a.61732

Lim, E. T., Uddin, M., De Rubeis, S., Chan, Y., Kamumbu, A. S., Zhang, X., D'Gama, A. M., Kim, S. N., Hill, R. S., Goldberg, A. P. et al. (2017). Rates, distribution and implications of postzygotic mosaic mutations in autism spectrum disorder. *Nat. Neurosci.* **20**, 1217-1224. doi:10.1038/nn.4598

Love, M. I., Huber, W. and Anders, S. (2014). Moderated estimation of fold change and dispersion for RNA-seq data with DESeq2. *Genome Biol.* **15**, 550. doi:10.1186/s13059-014-0550-8

Luche, H., Weber, O., Nageswara Rao, T., Blum, C. and Fehling, H. J. (2007). Faithful activation of an extra-bright red fluorescent protein in "knock-in" Cre-reporter mice ideally suited for lineage tracing studies. *Eur. J. Immunol.* **37**, 43-53. doi:10.1002/eji.200636745

Luo, W., Friedman, M. S., Shedden, K., Hankenson, K. D. and Woolf, P. J. (2009). GAGE: generally applicable gene set enrichment for pathway analysis. *BMC Bioinformatics,* **10**, 161. doi:10.1186/1471-2105-10-161

Machida, Y., Murai, K., Miyake, K. and Iijima, S. (2001). Expression of chromatin remodeling factors during neural differentiation. *J. Biochem.* **129**, 43-49. doi:10.1093/oxfordjournals.jbchem.a002834

Martynoga, B., Drechsel, D. and Guillemot, F. (2012). Molecular control of neurogenesis: a view from the mammalian cerebral cortex. *Cold Spring Harb. Perspect Biol.* **4**, a008359. doi:10.1101/cshperspect.a008359

Mashtalir, N., D'Avino, A. R., Michel, B. C., Luo, J., Pan, J., Otto, J. E., Zullow, H. J., McKenzie, Z. M., Kubiak, R. L., St Pierre, R. et al. (2018). Modular organization and assembly of SWI/SNF family chromatin remodeling complexes. *Cell*, **175**, 1272-1288.e20. doi:10.1016/j.cell.2018.09.032

Matsumoto, S., Banine, F., Feistel, K., Foster, S., Xing, R., Struve, J. and Sherman, L. S. (2016). Brg1 directly regulates Olig2 transcription and is required for oligodendrocyte progenitor cell specification. *Dev. Biol.* **413**, 173-187. doi:10.1016/j.ydbio.2016.04.003

Mercier, F. (2016). Fractones: extracellular matrix niche controlling stem cell fate and growth factor activity in the brain in health and disease. *Cell. Mol. Life Sci.* **73**, 4661-4674. doi:10.1007/s00018-016-2314-y

Mercier, F., Kitasako, J. T. and Hatton, G. I. (2002). Anatomy of the brain neurogenic zones revisited: fractones and the fibroblast/macrophage network. *J. Comp. Neurol.* **451**, 170-188. doi:10.1002/cne.10342

Moreno, N., Schmidt, C., Ahlfeld, J., Pöschl, J., Dittmar, S., Pfister, S. M., Kool, M., Kerl, K. and Schüller, U. (2014). Loss of Smarc proteins impairs cerebellar development. *J. Neurosci.* **34**, 13486-13491. doi:10.1523/JNEUROSCI.2560-14.2014

Narayanan, R. and Tuoc, T. C. (2014). Roles of chromatin remodeling BAF complex in neural differentiation and reprogramming. *Cell Tissue Res.* **356**, 575-584. doi:10.1007/s00441-013-1791-7

Pan, L., Yang, Z., Feng, L. and Gan, L. (2005). Functional equivalence of Brn3 POU-domain transcription factors in mouse retinal neurogenesis. *Development* **132**, 703-712. doi:10.1242/dev.01646

Panamarova, M., Cox, A., Wicher, K. B., Butler, R., Bulgakova, N., Jeon, S., Rosen, B., Seong, R. H., Skarnes, W., Crabtree, G. et al. (2016). The BAF chromatin remodelling complex is an epigenetic regulator of lineage specification in the early mouse embryo. *Development* **143**, 1271-1283. doi:10.1242/dev.131961

Roberts, C. W., Leroux, M. M., Fleming, M. D. and Orkin, S. H. (2002). Highly penetrant, rapid tumorigenesis through conditional inversion of the tumor suppressor gene Snf5. *Cancer Cell* **2**, 415-425. doi:10.1016/S1535-6108(02)00185-X

Saha, A., Tiwari, S., Dharmarajan, S., Otteson, D. C. and Belecky-Adams, T. L. (2018). Class I histone deacetylases in retinal progenitors and differentiating ganglion cells. *Gene Expr Patterns,* **30**, 37-48. doi:10.1016/j.gep.2018.08.007

Sekiguchi, F., Tsurusaki, Y., Okamoto, N., Teik, K. W., Mizuno, S., Suzumura, H., Isidor, B., Ong, W. P., Haniffa, M., White, S. M. et al. (2019). Genetic abnormalities in a large cohort of Coffin-Siris syndrome patients. *J. Hum. Genet.*, **64**, 1173-1186. doi:10.1038/s10038-019-0667-4

Sen, P., Luo, J., Hada, A., Hailu, S. G., Dechassa, M. L., Persinger, J., Brahma, S., Paul, S., Ranish, J. and Bartholomew, B. (2017). Loss of Snf5 Induces Formation of an Aberrant SWI/SNF Complex. *Cell Rep* **18**, 2135-2147. doi:10.1016/j.celrep.2017.02.017

Seo, S., Richardson, G. A. and Kroll, K. L. (2005). The SWI/SNF chromatin remodeling protein Brg1 is required for vertebrate neurogenesis and mediates transactivation of Ngn and NeuroD. *Development* **132**, 105-115. doi:10.1242/dev.01548

Singh, A. P., Foley, J. F., Rubino, M., Boyle, M. C., Tandon, A., Shah, R. and Archer, T. K. (2016). Brg1 enables rapid growth of the early embryo by suppressing genes that regulate apoptosis and cell growth arrest. *Mol. Cell. Biol.* **36**, 1990-2010. doi:10.1128/MCB.01101-15

Smith, A. N., Miller, L.-A., Radice, G., Ashery-Padan, R. and Lang, R. A. (2009). Stage-dependent modes of Pax6-Sox2 epistasis regulate lens development and eye morphogenesis. *Development* **136**, 2977-2985. doi:10.1242/dev.037341

Sokpor, G., Castro-Hernandez, R., Rosenbusch, J., Staiger, J. F. and Tuoc, T. (2018). ATP-Dependent chromatin remodeling during cortical neurogenesis. *Front. Neurosci.* **12**, 226. doi:10.3389/fnins.2018.00226

Son, E. Y. and Crabtree, G. R. (2014). The role of BAF (mSWI/SNF) complexes in mammalian neural development. *Am. J. Med. Genet. C Semin. Med. Genet.* **166c**, 333-349. doi:10.1002/ajmg.c.31416

Sumi-Ichinose, C., Ichinose, H., Metzger, D. and Chambon, P. (1997). SNF2beta-BRG1 is essential for the viability of F9 murine embryonal carcinoma cells. *Mol. Cell. Biol.* **17**, 5976-5986. doi:10.1128/MCB.17.10.5976

Tang, K., Xie, X., Park, J. I., Jamrich, M., Tsai, S. and Tsai, M. J. (2010). COUP-TFs regulate eye development by controlling factors essential for optic vesicle morphogenesis. *Development* **137**, 725-734. doi:10.1242/dev.040568

Tsurusaki, Y., Okamoto, N., Ohashi, H., Kosho, T., Imai, Y., Hibi-Ko, Y., Kaname, T., Naritomi, K., Kawame, H., Wakui, K. et al. (2012). Mutations affecting components of the SWI/SNF complex cause Coffin-Siris syndrome. *Nat. Genet.* **44**, 376-378. doi:10.1038/ng.2219

Wang, W., Cote, J., Xue, Y., Zhou, S., Khavari, P. A., Biggar, S. R., Muchardt, C., Kalpana, G. V., Goff, S. P., Yaniv, M. et al. (1996). Purification and biochemical heterogeneity of the mammalian SWI-SNF complex. *EMBO J.* **15**, 5370-5382. doi:10.1002/j.1460-2075.1996.tb00921.x

Weider, M., Kuspert, M., Bischof, M., Vogl, M. R., Hornig, J., Loy, K., Kosian, T., Muller, J., Hillgartner, S., Tamm, E. R. et al. (2012). Chromatin-remodeling factor Brg1 is required for Schwann cell differentiation and myelination. *Dev. Cell* **23**, 193-201. doi:10.1016/j.devcel.2012.05.017

West-Mays, J. A., Zhang, J., Nottoli, T., Hagopian-Donaldson, S., Libby, D., Strissel, K. J. and Williams, T. (1999). AP-2alpha transcription factor is required for early morphogenesis of the lens vesicle. *Dev. Biol.* **206**, 46-62. doi:10.1006/dbio.1998.9132

Yates, A. D., Achuthan, P., Akanni, W., Allen, J., Allen, J., Alvarez-Jarreta, J., Amode, M. R., Armean, I. M., Azov, A. G., Bennett, R. et al. (2020). Ensembl 2020. *Nucleic Acids Res.* **48**, D682-D688. doi:10.1093/nar/gkz966

Yu, G. and He, Q. Y. (2016). ReactomePA: an R/Bioconductor package for reactome pathway analysis and visualization. *Mol. Biosyst.* **12**, 477-479. doi:10.1039/C5MB00663E

Zhao, S., Thornquist, S. C. and Barnstable, C. J. (1995). In vitro transdifferentiation of embryonic rat retinal pigment epithelium to neural retina. *Brain Res.* **677**, 300-310. doi:10.1016/0006-8993(95)00163-K

Zhu, Y., Li, D., Wang, Y., Pei, C., Liu, S., Zhang, L., Yuan, Z. and Zhang, P. (2015). Brahma regulates the Hippo pathway activity through forming complex with Yki-Sd and regulating the transcription of Crumbs. *Cell. Signal.* **27**, 606-613. doi:10.1016/j.cellsig.2014.12.002